**The Role of Ring Strain in the Reactivity of Transition Metal-Catalyzed
C–C Bond Activation Reactions**

by

Tyler Mark Ahlstrom

BA Philosophy, University of Minnesota, 2011

PhD History and Philosophy of Science, University of Pittsburgh, 2019

Submitted to the Graduate Faculty of the

Dietrich School of Arts and Sciences in partial fulfillment

of the requirements for the degree of

Master of Science

University of Pittsburgh

2022

UNIVERSITY OF PITTSBURGH

DIETRICH SCHOOL OF ARTS AND SCIENCES

This thesis was presented

by

Tyler Mark Ahlstrom

It was defended on

January 20, 2022

and approved by

Tara Meyer, Professor, Department of Chemistry

Geoffrey Hutchison, Associate Professor, Department of Chemistry

Thesis Advisor: Peng Liu, Associate Professor, Department of Chemistry

**The Role of Ring Strain in the Reactivity of Transition Metal-Catalyzed
C–C bond activation reactions**

Tyler Mark Ahlstrom, MS

University of Pittsburgh, 2022

Thesis abstract: Cyclic alkanes and ketones are common starting materials in transition metal-catalyzed C–C bond activation reactions because their ring strain provides the thermodynamic driving force of the otherwise challenging C–C bond cleavage step. A computational study was performed to investigate the factors affecting the thermodynamics and kinetics of transition-metal-catalyzed C–C bond activation reactions of cyclic alkanes and ketones. The results show that while the reaction energies and rates are strongly affected by the release of ring strain and, in the case of ketones, metal-carbonyl back-bonding, the rates are also affected by steric environment of the C–C bond prior to activation. Linear structure-activity relationships are explored for these factors and quantitatively compared for Ni-, Rh-, and Ir-based catalysts, and for cyclic reactants with three-, four-, and five-membered rings.

Table of Contents

List of Figures

1.0 Introduction & Background

The activation of C–C bonds promoted by transition metal catalyst has increasingly proven to be a broad and valuable tool for the discovery of novel synthetic pathways.[1–8] The insertion of a transition metal into a C–C bond enables a wide range of subsequent functionalization pathways for the resulting organometallic intermediates. Given the general availability of C–C bonds in organic compounds, this technique enables synthetic pathways utilizing readily available yet relatively inert starting materials not accessible by traditional methods. While Tipper first reported activating cyclopropane using a Pt complex in 1955, the past decade has shown advances using a variety of other transition metal catalysts, especially Pd, Rh, Ru, and Ni, and less strained four- and five-membered ring starting materials.[9–19] C–C activation has been achieved via several different mechanism, including β-carbon elimination [20] and retro-allylation [21], but the present work will focus exclusively on the most common approach: oxidative addition. Figure 1 shows a generic C–C cleavage via oxidative addition to a transition metal catalyst, and subsequent functionalization via migratory insertion and reductive elimination.
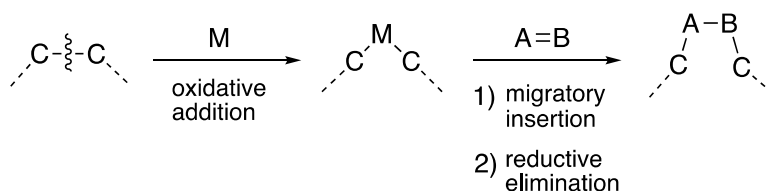
Figure 1: Generic C–C cleavage via oxidative addition

The primary barrier to these reactions is the cleavage of the C–C bond, which is unfavorable for both kinetic and thermodynamic reasons. In addition to being stronger than C–M bonds, the σ-orbital of a

C−C bond is highly directional, reducing its potential for overlap with the frontier orbitals of a metal catalysts, and its HOMO is typically too low (and LUMO too high) for significant interaction even if proper geometry were achieved. Additionally, although C−H bonds are stronger than C−C bonds in terms of bond dissociation energies, many transition metal complexes preferentially undergo oxidative addition with C−H bonds, which are much less crowded than C−C bonds.

There are several strategies for overcoming the inertness of C–C bonds, including the use of directing groups or carbon-cyano starting materials, but the most widespread is the use of strained cyclic starting materials. Figure 2 (a) shows the use of Wilkinson's catalyst to form rhodaindanone via C–C bond cleavage of benzocyclobutenone, an activation pathway discovered by Liebeskind and co-workers in 1992, and recently used by the Dong group to achieve a wide variety of subsequent C−C forming reaction pathways.[22–24] For example, Figure 2 (b) shows the intramolecular insertion of an olefin into the C1-C2 bond of benzocyclobutenones, which can achieve significantly better conversion and yield than Wilkinson's catalyst after optimizing the ligands.[25] The activation of C−C bonds in strained starting materials has also been achieved with several other transition metals, including Ir (Figure 2, c)[26] and Ni (Figure 2, d)[6].

a) C–C bond activation of benzocyclobutenone using Wikinson's catalyst
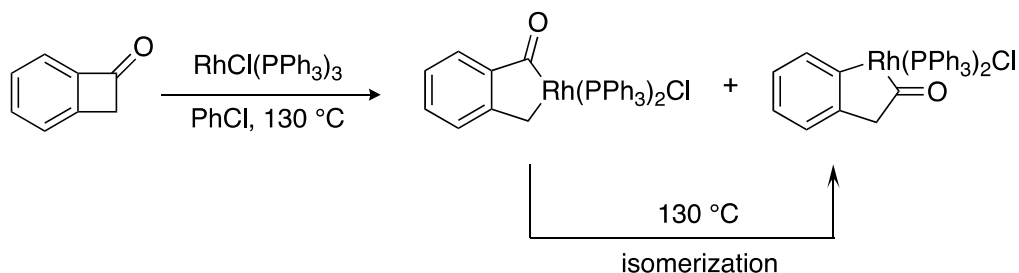
b) Carboacylation of olefin via the C–C bond cleavage of benzocyclobutenone by a dppm-supported Rh catalyst
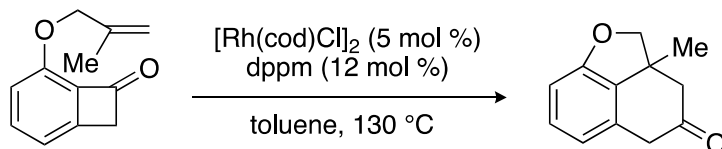
c) Pyrazole synthesis using DG and Ir catalyst
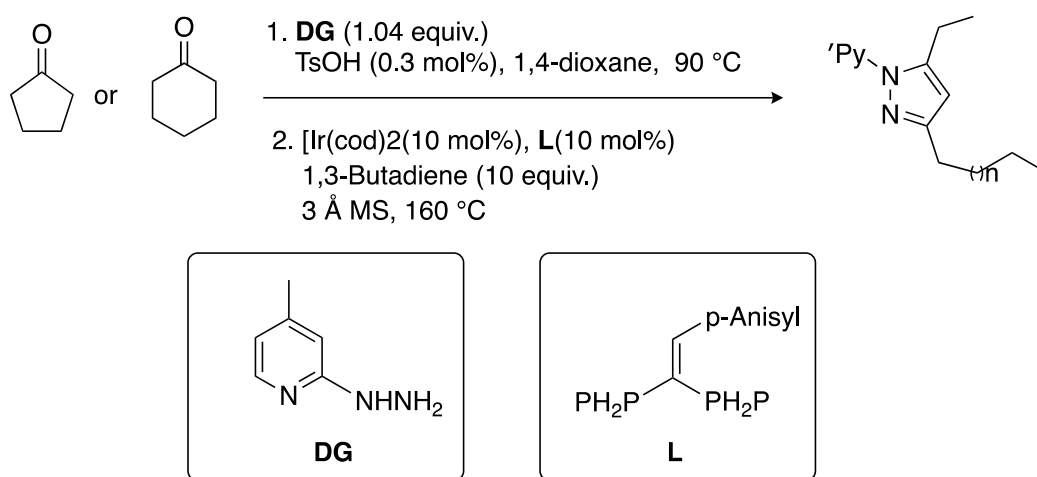
d) C-1 insertion of isocyanides into Biphenylene using a Ni catalyst
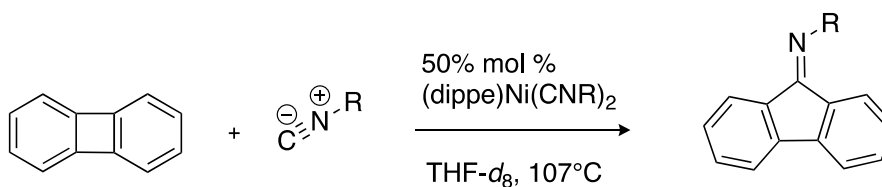
Figure 2: Examples of C–C bond activation using Rh (a,b), Ir (c), and Ni (d)

While the use of strained cyclic reactants facilitates C–C activation, there remains debate about the precise role of strain. Specifically, it has not been conclusively shown whether it is the strain of the reactant itself that facilitates the oxidative addition, or alternatively, whether it is the magnitude of ring

strain release, *i.e.* the decrease of ring strain in the reactant and the larger metallacycle, that facilitates the reaction. Additionally, it is common to have cyclic ketones as the reactants of these reactions, but the origin of their reactivity difference compared with cyclic alkanes—including how it may complicate the foregoing question about the role of strain—remains unexplored. Having a better understanding of these factors would aid the exploration of this new area of research by helping to predict whether a proposed cleavage is feasible and under what conditions it might occur.

To answer these questions, a systematic exploration of the factors affecting both the thermodynamics and kinetics of the C–C cleavage is undertaken. A total of 18 ring-opening oxidative addition reactions are examined, covering reactions proceeding from reactants with different ring sizes (3, 4, and 5 membered rings) with and without a carbonyl group, as well as three different representative transition metal catalysts: $Ni(PPh_3)_2$, $Rh(dppm)Cl$, and $Ir(dppm)Cl$ (Figure 3). These model reactions were selected in part because some of them feature prominently in the literature, but primarily because trends in the thermodynamics and kinetics of these reactions are expected to probe the foregoing questions about the role of strain and the effect of the carbonyl group.
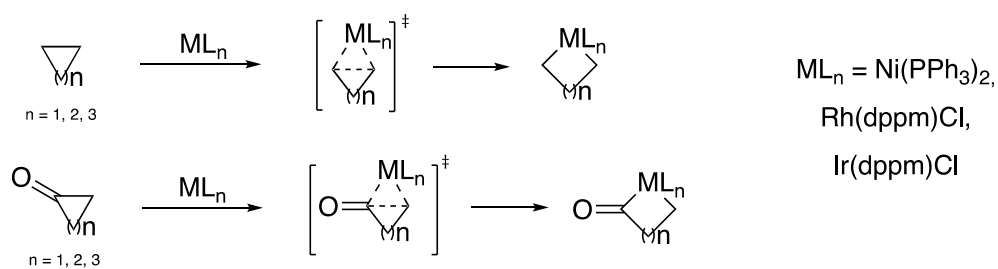
Figure 3: C–C cleavage of strained cyclic alkanes and ketones via oxidative addition

In all explored reactions, a cyclic reagent (either a cycloketone or cycloalkane) is added via oxidative addition to a transition metal, thereby expanding the size of the ring, and to some extent relieving the strain of the reagent. This work probes the role of strain in these reactions, quantifying and identifying trends in the strain of the reagent as well as the release of strain over the course of this oxidative addition.

2.0 Computational Methods

The B3LYP[27–29] density functional and a mixed basis set of LANL2DZ[30–32] for metals and 6-31G(d)[33–39] for other atoms were used in geometry optimizations. Vibrational frequencies were calculated at the same level of theory as geometry optimization. All minima, including starting materials and products, have zero imaginary frequency. All transition states have one imaginary frequency. Single-point energies were calculated with M06[40] and a mixed basis set of SDD[41–56] for metals and 6-311+G(d,p)[57,58] for other atoms. Solvation energy corrections were calculated in single-point energy calculations using the SMD[59,60] model with THF solvent. Gibbs free energies and enthalpies include thermal corrections calculated at 298.15 K and 1.0 atmospheres using the standard procedures in Gaussian.[61] All DFT calculations were performed using Gaussian 16.[62] Atomic charges were calculated using natural bonding orbitals.[63]

2.1 Homodesmotic calculation of ring strain

Experimentally, ring strain is usually calculated using heats of combustion, and specifically by comparing the heat of combustion of the cyclic structure to that of an appropriate linear structure.[64] However, there are two major problems with this experimental approach for the current investigation. First, while hydrocarbons combust in straightforward manner to form well defined and obtainable products, this is less often the case with the more complex structures explored in this work. And second, the experimental approach requires being able to first isolate the structures in workable purity and quantity, and as all of the metallacycles explored in this work are reactive intermediates, it would

be exceedingly difficult to satisfy this precondition (this applies as well to the corresponding linear structures needed to calculate ring strain). As such, we will be exploring ring strain computationally.

All ring strain energies were calculated using a homodesmotic reaction equation.[65,66] Homodesmotic reactions are a subclass of isodesmic reactions, where the reactants and products contain the same number and type of bonds, the same number of hybridization states for each element, and the same number of primary, secondary, etc. carbons.[67,68] For example, below (Figure 4) are the equations used to calculate the ring strain energy (ΔH_{RSE}) of cyclobutane, cyclobutanone, and the corresponding 4-membered metallacycles.

$$\Delta H_{\mathrm{RSE}} = -\Delta H_{\mathrm{rxn}}$$
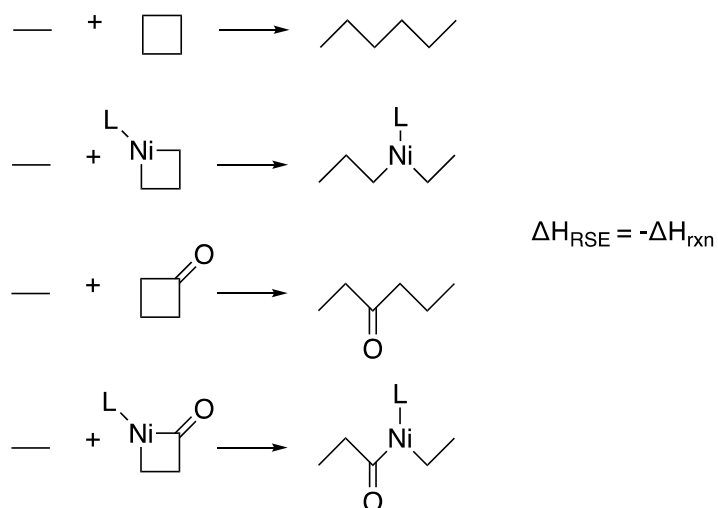
Figure 4: Homodesmotic ring strain calculations

Each of the above are examples of homodesmotic ring strain calculations that were used in this work to determine the ring strain of the above metallacycles. Note both sides of each 'reaction' contain the same number of each type of bond, as well as the same number of primary and secondary carbons.

Each scheme in Figure 4 is an isodesmic reaction in that both sides contain the same number and type of bonds, and they are furthermore homodesmotic because both sides contain the same number of hybridization state for each element and the same number of primary, secondary, etc. carbons. Ring strain energies calculated using homodesmotic reactions are reliable due to cancellation of model error[68] and because they take into account corrections due 1,3-alkyl-alkyl interaction or 'protobranching'.[69] For additional criteria leading to even more accurate RSE calculations, see ref. [68]. For our purposes, homodesmotic reactions were chosen to quantify ring strain because they are sufficiently accurate and are broadly accepted in the literature.[68,70–72] Furthermore, any error due to uncaptured protobranching or other sources of error will be present in all ring strain calculations, and therefore not relevant to the trends across the different systems, which is our primary concern.

Note that ring strain of cyclic compounds may be due to the combination of several different types of distortion effects. More specifically, there will be several differences between the two sides of the homodesmotic reaction equation, and it is the sum of these differences that is being grouped together as 'ring strain energy'. For example, the cyclic molecules will often have longer, weaker bonds, decreased hyperconjugation, and a variety of other differences. Where a more detailed computational analyses may seek to distinguish these several factors, and identify the dominant one or a couple for 'ring strain energy', here we will regard the entire set of differences as factors that together quantify ring strain energy. This approach allows for a more straightforward and reliable quantification of ring strain energy, and also generates results that are more relevant to the synthetic practices explored above.

3.0 Oxidative Addition with Cyclic Ketones

Cyclic ketones will be explored first because they are more commonly used starting materials with relatively less strained rings. Experimentally, four-, and five-membered cyclic ketones have been effectively activated using transition metal catalysts. On the other hand, although three-membered cyclic alkanes (cyclopropanes) are often used in C–C bond cleavage reactions, the activation of four- and five-membered cyclic alkanes are rare. The reactivities of cyclic ketones will be examined in Chapter 4.

3.1 Thermodynamics of oxidative addition with cyclic ketones

The formation of nine metallacycles via oxidative addition of cyclic ketones were analyzed, three for each transition metal catalyst included in this research—$Ni(PPh_3)_2$, $Rh(dppm)Cl$, and $Ir(dppm)Cl$ (see Figure 5 and Figure 6 for details). In order to determine the role of strain energy in the formation of these complexes, cyclic ketones of varying size were used, including cyclopropanone, cyclobutanone, and cyclopentanone.
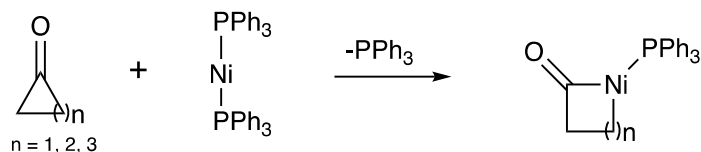
Figure 5: Cyclic ketone oxidative addition with a Ni catalyst

The oxidative addition of three cyclic ketones with an Ni-based catalyst were examined, corresponding to n = 1, 2, and 3. The Ni reagents are supported by two PPh_3 ligands, chosen due to its common use with Ni. One PPh_3 ligand is dissociated from the Ni during the formation of the metallacycles in order to avoid significant steric interaction between the ligands and the metallacycle.
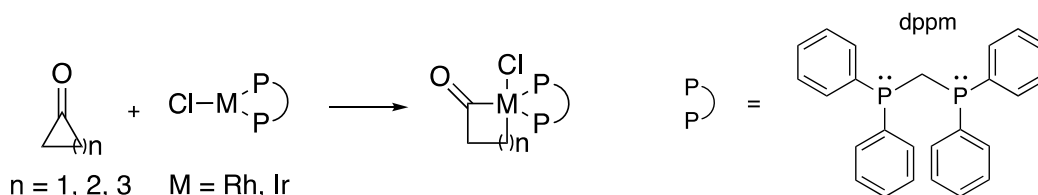
Figure 6: Cyclic ketone oxidative addition with Rh and Ir catalysts

For each Rh and Ir catalyst, the formation of three metallacycles via oxidative addition were examined. Bis(diphenylphosphino)methane (dppm)-supported Rh(I) and Ir(I) chloride complexes were chosen again due to their use in the literature. Note that dppm is a bidentate ligand and both phosphorus atoms remain coordinated to the metal center in both the starting material and metallacycle.

Figure 7 shows the reaction Gibbs free energies (Δ*G)* of the formation of nine different metallacycles: each of three cyclic ketones undergoing oxidative addition with each of three different transition metal catalysts. Two trends are immediately visible. First, given a transition metal catalyst, the oxidative addition of ketones with smaller ring size leads to thermodynamically more favorable reactions.

Second, given a cyclic ketone, the thermodynamic preference proceeds in the order Ir > Rh > Ni.

These two trends will now be explored in turn.
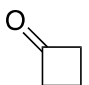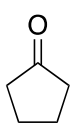
	NiPPh$_3$	RhCl(dppm)	IrCl(dppm)
O (n = 1)	-1.7	-18.1	-28.5
O (n = 2)	5.7	-8.1	-18.7
O (n = 3)	23.5	10.5	-1.7

Figure 7: Reaction Gibbs free energies (ΔG, kcal/mol) of oxidative addition with cyclic ketones

The Gibbs free energy (ΔG, kcal/mol) of metallacycle formation (following schemes shown in Figure 5 and Figure 6) showing two trends: i) for a given transition metal catalyst, the oxidative addition of ketones with smaller ring size is more thermodynamically favorable, and ii) for a given cyclic ketone, the thermodynamic preference proceeds in the order Ir > Rh > Ni. The Gibbs free energies are with respect to the cyclic ketone and transition metal complex (Ni(PPh$_3$)$_2$, Rh(dppm)Cl, or Ir(dppm)Cl). Note that for the reactions with Ni(PPh$_3$)$_2$, the resulting metallacycle product has a PPh$_3$ ligand dissociated from the metal (see Figure 5).

To understand the greater reactivity of smaller ketone rings, homodesmotic ring strain calculations were performed on both the cyclic ketone reactants and the metallacycles that result from their

oxidative addition with the three transition metal catalysts (see section 2.1 for discussion of homodesmotic calculations). Figure 8 shows the results of these calculations. Although the ring strain energies of cyclic ketones have been extensively studies and are often considered as the primary driving force for C–C bond cleavage, the effects of ring strain of the resulting metallacycle intermediates are often overlooked. For a given metal, the five-membered metallacycle (n = 2) is the least strained, and the four-membered metallacycle (n = 1) the most strained. This trend is also corroborated by bond angle considerations. Interestingly, for a given size of metallacycle, there is relatively little to distinguish the ring strain across the different metals; while the Rh metallacycles are slightly less strained, the difference is marginal.
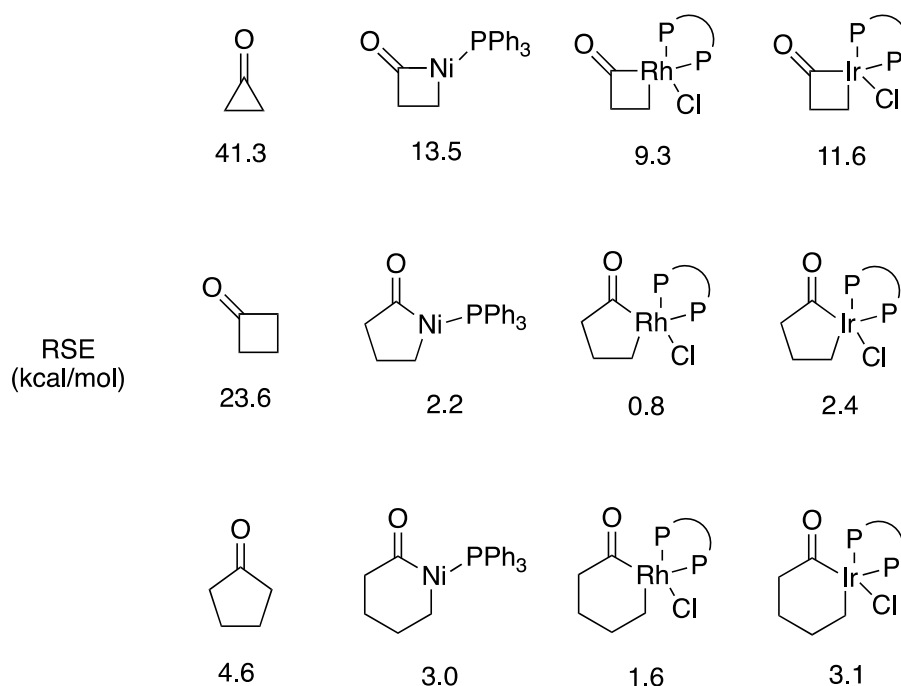
Figure 8: Ring strain energies of cyclic ketones and metallacycles

All ring strain energies (kcal/mol) are calculated using a homodesmotic calculation (see section 2.1). No significant interaction between these ligands and the metallacycle was present; see appendix Figure 39 details.

When we turn our attention to the ring strain released (RSR) through the reaction—the difference between the ring strain of the metallacycle and the cyclic ketone reactant—there is a strong linear relationship with the ΔG_{rxn} (Figure 10). This strong linear relationship ($r^2 >= 0.99$) with a slope near 1 suggests that RSR is an independent driving force for the formation of these metallacycles. While there is also a strong linear relationship between ΔG_{rxn} and the strain of the starting reagent (Figure 9), this is to be expected given that RSR and the initial ring strain are highly correlated (appendix Figure 33.
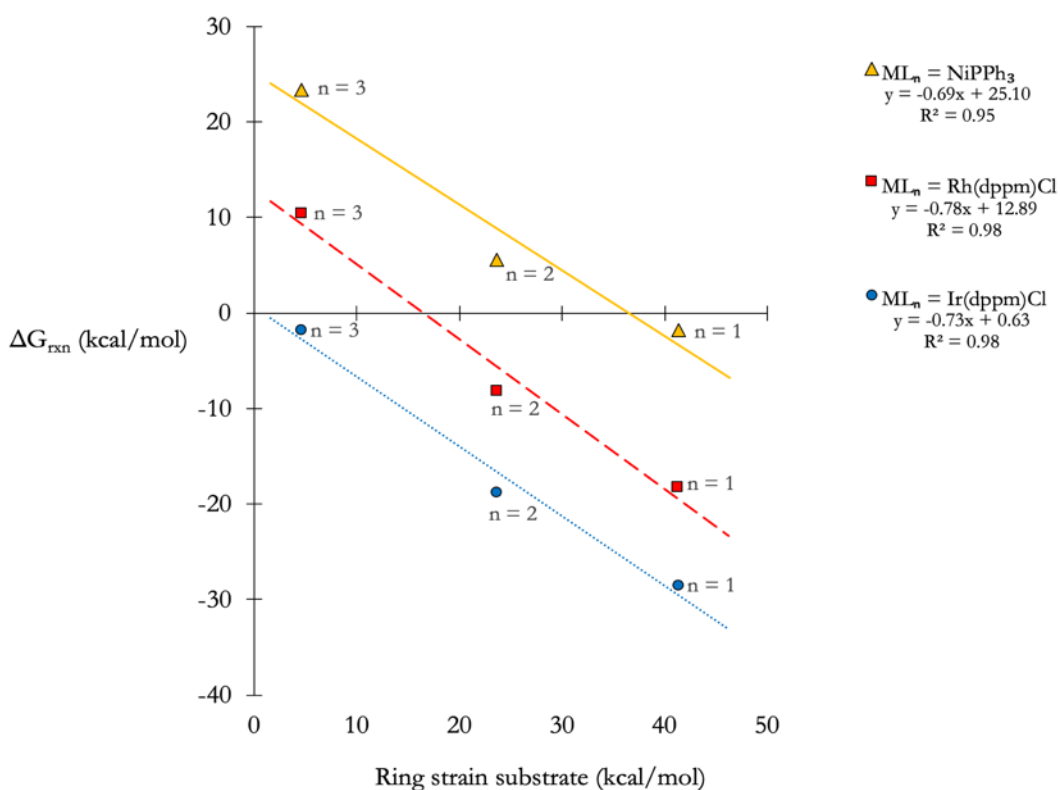
Figure 9: Ring strain substrate vs ΔG_{rxn} for the oxidative addition of cyclic ketones

The ring strain of the substrate (kcal/mol) vs. ΔG_{rxn} (kcal/mol) of the cyclic ketone oxidative addition. Again, 'n' corresponds to the size of the ketone reactant (see Figure 5 and Figure 6) with n = 1, 2, 3 corresponding to a three-, four-, and five-membered ketones. The linear relationship remains strong, though not quite as strong as Figure 10.
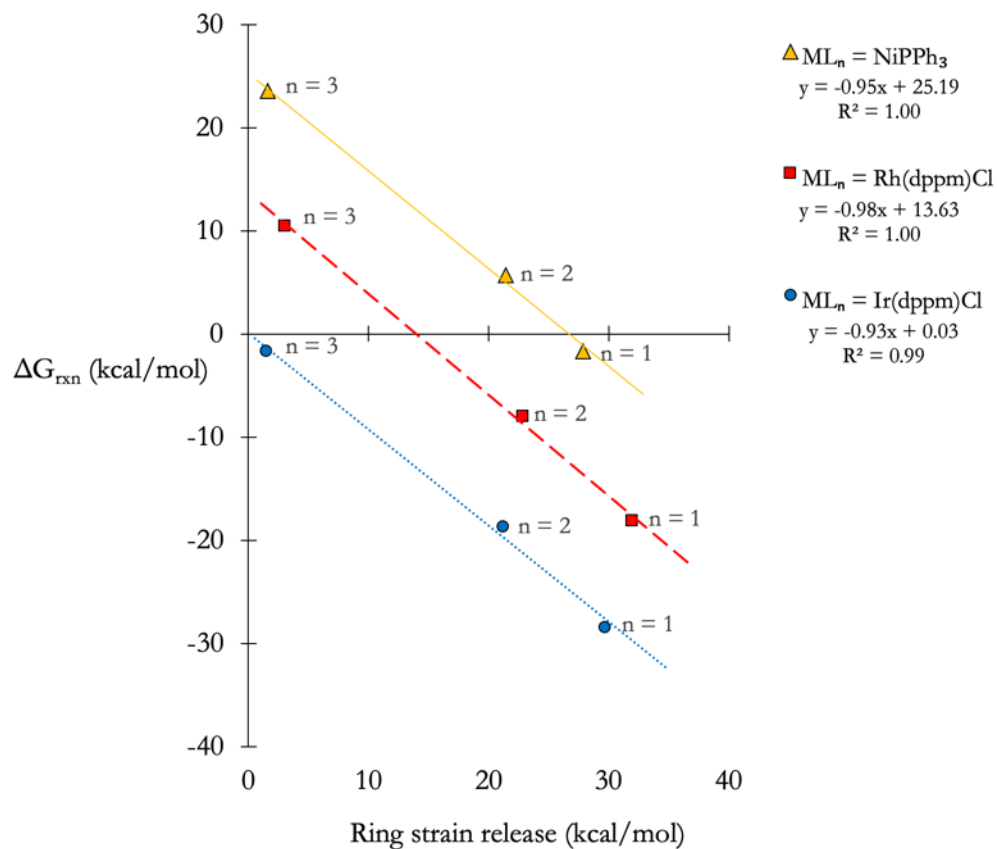
Figure 10: Ring strain release vs ΔG_{rxn} for the oxidative addition of cyclic ketones

The ring strain released (kcal/mol) vs. ΔG_{rxn} (kcal/mol) of the cyclic ketone oxidative addition. 'n' corresponds to the ring size of the ketone reactant (see Figure 5 and Figure 6) with n = 1, 2, 3 corresponding to a three-, four-, and five-membered ketones. The strong linear relationship with a slope near 1 suggests ring strain release is an independent driving force of the reaction.

The gaps between the linear fits for the different metals in Figure 9 brings us back to our second task: to explain the reactivity of the different metals, and specifically why their reactivity proceeds in the

order Ir > Rh > Ni. It was hypothesized that this was due to varying amounts of metal-carbon backbonding that donates electron from the metal d orbital to the π^* orbital of carbonyl, with Ir most able to engage in backbonding, and Ni the least able. To explore this, bond dissociation energies were calculated and a natural bonding orbital (NBO) analysis was performed (Figure 11). The comparison between the BDEs of C(ethyl)–M and C(acyl)–M for the different metals indicates that the C(acyl)–M bond with Rh and Ir are stronger than the corresponding C(ethyl)–M bond, likely due to the stronger backdonation in C(acyl)–M whereas the C(acyl–Ni bond is weaker than C(ethyl)–Ni, suggesting the C(acyl)–Ni is weaker. The $\pi^*(C=O)$ occupancy from NBO calculations provides further insights into the magnitude of backdonation with the different metals. The $\pi^*(C=O)$ occupancy suggests the same trend: Ir > Rh > Ni. The NPA atomic charge of the O atom likewise supports this trend, but for unknown reasons the C=O frequency does not (see appendix Figure 35).
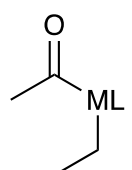
	ML = Ni(PPh₃)	Rh(dppm)Cl	Ir(dppm)Cl
Et—ML BDE (kcal/mol)	57.9	57.6	68.1
$CH_3C(O)$—ML BDE (kcal/mol)	54.5	63.9	73.1
C=O π^* NBO occupancy (e⁻)	0.127	0.143	0.178

Figure 11: Evidence of backdonation from metal to C=O π* orbital

The metal-carbon bond dissociation energies (BDEs) and C=O π^* occupancy for the three different metal complexes were examined. The trend present in both measurements corroborates the Ir > Rh > Ni ordering with regards to their ability to engage in backdonation. Note that there were no significant changes in these values for different alkyl or acyl groups with different carbon chain lengths (corresponding to different 'n' in Figure 7). Also note the carbon-metal bonds are all weaker than carbon-carbonyl bonds (~75 kcal/mol), and will be outcompeted by most ligands; the formation of these bonds is not a thermodynamic driver.

3.2 Kinetics of cyclic ketone oxidative addition

Transition states were located for all oxidative addition reactions detailed in Figure 12 and Figure 13. All activation Gibbs free energies are shown in Figure 14. Again the more strained reactants (especially cyclopropanone) are more reactive. However, here there is no neat trend separating the reactivities of the different metal complexes; the identity of the metal itself appears to affect $\Delta G^{\ddagger}$ very little. This

suggests that Ni, despite being a first-row metal, may nonetheless be used as an effective catalyst for C–C cleavage.
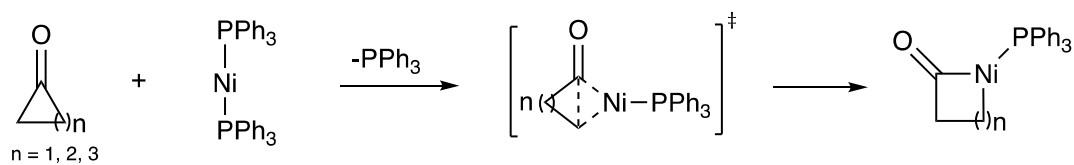
Figure 12: Transition state of cyclic ketone oxidative addition with a Ni catalyst
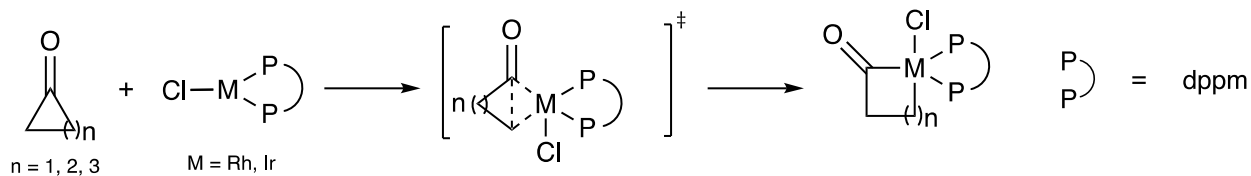
Figure 13: Transition state of cyclic ketone oxidative addition with Rh- and Ir-based catalysts
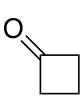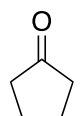
	NiPPh$_3$	RhCl(dppm)	IrCl(dppm)
O ⊿ n = 1	16.5	9.9	10.9
O ▢ n = 2	18.1	17.3	16.2
O ⬠ n = 3	25.7	25.9	23.0

Figure 14: $\Delta G^{\ddagger}$ (kcal/mol) of oxidative addition of cyclic ketones

The $\Delta G^{\ddagger}$ (kcal/mol) of metallacycle formation via oxidative addition (following Figure 12 and Figure 13) showing the more strained reactants to be more reactive. The activation free energies are with respect to the cyclic ketone and transition metal complex (Ni(PPh$_3$)$_2$, Rh(dppm)Cl, or Ir(dppm)Cl). Note again that for the reactions with Ni(PPh$_3$)$_2$, the resulting metallacycle product has a PPh$_3$ ligand dissociated from the metal (see Figure 12).

Figure 15 shows that each series displays an approximately linear relationship between ΔG_{rxn} vs $\Delta G^{\ddagger}$, suggesting that the reaction kinetics is governed by the Bell–Evans–Polanyi principle. This is corroborated by an examination of the transition states (Rh transition states shown in Figure 16). There is a clear trend of a later transition state as the size of the cyclic reagent increase, which is expected given that the reactions also become less exothermic (Hammond postulate; the percentage change of C–C bond length at the TS is confirms this trend as well, plotted in Appendix Figure 37). The same trend was observed with Ni and Ir.
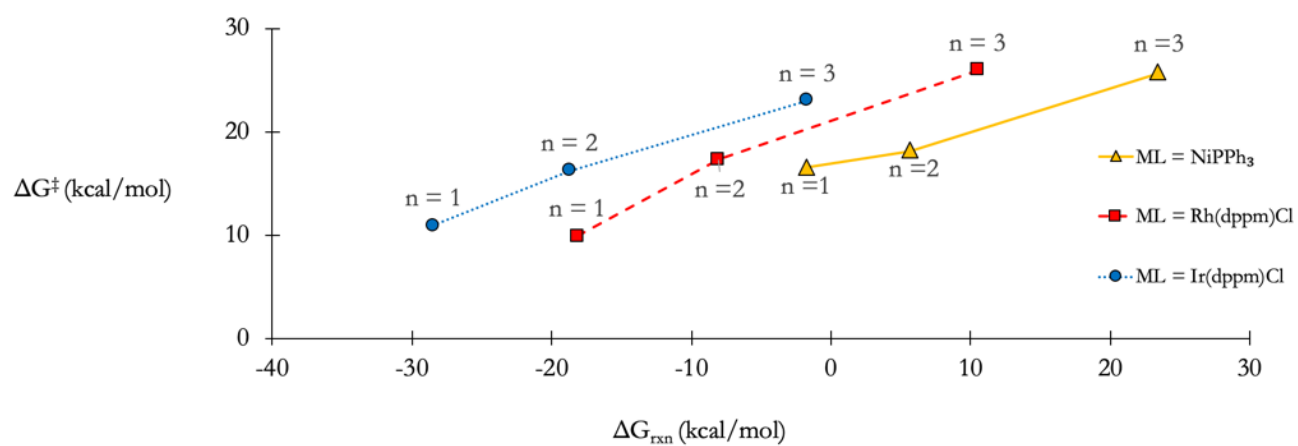
18

Figure 15: ΔG_{rxn} vs $\Delta G^{\ddagger}$ of oxidative addition of cyclic ketones

The linear relationship between ΔG_{rxn} and $\Delta G^{\ddagger}$ suggest that the reactivity of oxidative addition is affected by the reaction free energies.
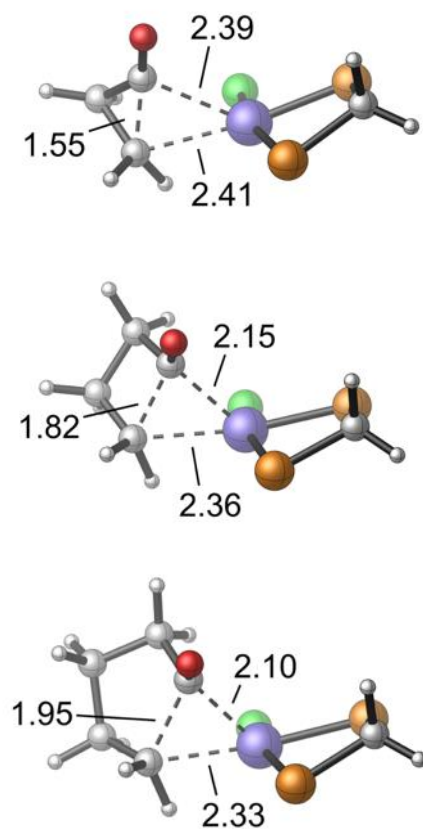
Figure 16: Transition states of the oxidative addition of cyclic ketones using and Rh(I) catalyst

There is a clear trend of a later transition state as the size of the cyclic reagent increases, with the length of the breaking C–C bond increasing and the length of the forming C–Rh bonds decreasing at the transition states for the larger ringed systems.

The role of ring strain in the energetics of the transition states were explored. Figure 17 shows a strong correlation between $\Delta G^{\ddagger}$ and the ring strain of the cyclic reagent, and Figure 18 shows a strong correlation between $\Delta G^{\ddagger}$ and the ring strain released over the course of the complete reaction. It is difficult to say whether reagent ring strain or ring strain release drives the kinetics more than the other, but this is not too surprising given the strong correlation between the two (plotted in Appendix Figure 33). The relatively low slope of both graphs indicate that C–C activation is feasible with only

20

moderately strained ketones, including cyclopentanone as reported here, and even cyclohexanone.[73] The question of how much strain energy is released by the transition state was ultimately set aside due to difficulties quantifying TS strain energy in a way that is consistent and meaningful across the different systems.
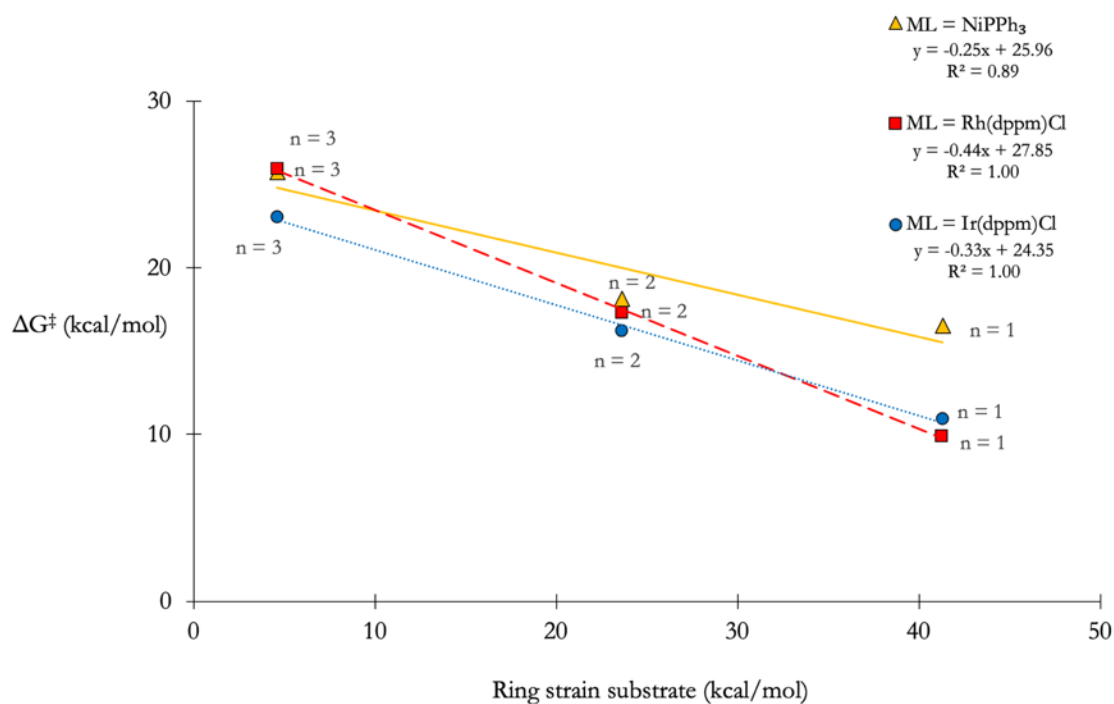
Figure 17: Ring strain of substrate vs ΔG‡

The transition state energies are strongly correlated with the ring strain of the starting cyclic ketones.
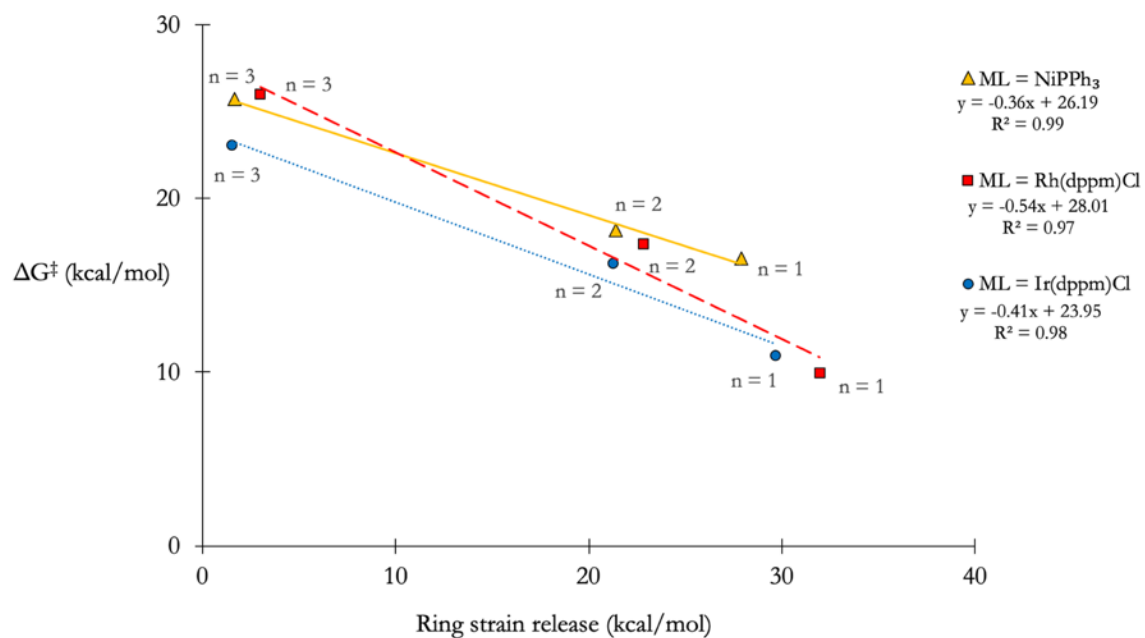
Figure 18: Ring strain release of reaction vs ΔG‡

The transition state energies are also strongly correlated with the ring strain release (RSR) of the reaction. Note that this RSR is for the complete reaction; ring strain release was not calculated at the transition state itself.

4.0 Oxidative Addition with Cyclic Alkanes

A parallel analysis was done using cyclic alkanes rather than cyclic ketones. While oxidative addition using various sized cyclic ketones is common, oxidative addition with cyclic alkanes has focused largely on cyclopropane. While it is well documented that cyclopropane has exceptional properties[74], this work details how they manifest in the context of oxidative addition. Mirroring the exploration above, the oxidative addition of nine cyclic alkanes were analyzed, three for each transition metal catalyst included in this research. This affected several of the trends found with the cycloketone reagents.

4.1 Thermodynamics of oxidative addition with cyclic ketones

In order to determine the role of strain energy in the formation of these complexes, cyclic alkanes of varying size were used, including cyclopropane, cyclobutane, and cyclopentane (Figure 19 and Figure 20).
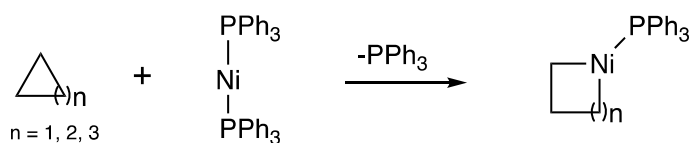
Figure 19: Cyclic alkane oxidative addition with a Ni catalyst

The oxidative addition of three cyclic alkanes with an Ni-based catalyst were examined, corresponding to n = 1, 2, 3. The same metal ligands are used as with the ketones above. Again, one PPh_3 ligand is dissociated from the Ni during the formation of the Ni metallacycles in order to avoid significant steric interaction between the ligands and the metallacycle.

$$\triangle \!\!\!)_n \quad + \quad Cl\!-\!M\!\!\begin{array}{c}P\\P\end{array}\!\!) \quad \longrightarrow \quad \square \!\!\!)_n \!-\! \overset{\overset{Cl}{|}}{M}\!\!\begin{array}{c}P\\P\end{array}\!\!) \qquad \begin{array}{c}P\\P\end{array}\!\!) \ = \ dppm$$

n = 1, 2, 3   M = Rh, Ir
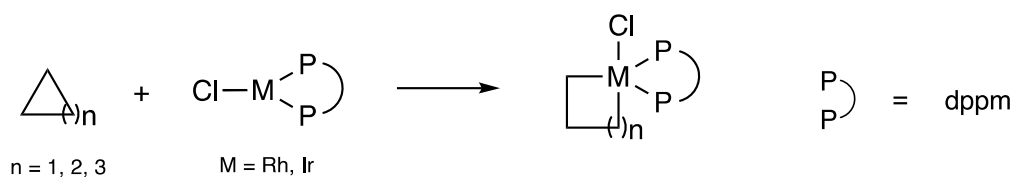
Figure 20: Cyclic alkane oxidative addition with Rh and Ir catalysts

For each Rh and Ir catalyst, the formation of three metallacycles were examined. Bis(diphenylphosphino)methane (dppm)-supported Rh(I) and Ir(I) chloride complexes were chosen again due to their use in the literature. Note that dppm is a bidentate ligand and both phosphorus atoms remain coordinated to the metal center in both the starting material and metallacycle.

Figure 21 shows the reaction Gibbs free energies (ΔG_{rxn}) for all nine oxidative addition reactions. Unlike the corresponding reactions involving cyclic alkanes above, reactions with smaller cyclic reactants are not always more thermodynamically favorable. Given a transition metal catalyst, oxidative addition with cyclobutane (n = 2) is the most thermodynamically favorable, and oxidative addition with cyclopentane (n = 3) is least thermodynamically favorable. When we compare the reactivity of the different metal catalysts, the same trend is observed as with the cyclic ketones: given a cyclic alkane, the thermodynamic preference proceeds in the order Ir > Rh > Ni. Overall, these reactions are much less thermodynamically favorable than oxidative addition with the corresponding cyclic ketone; only the reaction of cyclobutane with IrCl(dppm) is exothermic.
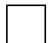
	NiPPh$_3$	RhCl(dppm)	IrCl(dppm)
△ n = 1	18.6	11.3	1.1
☐ n = 2	13.1	3.3	-7.0
⬠ n = 3	29.8	24.1	14.1

Figure 21: Reaction Gibbs free energies (ΔG, kcal/mol) of oxidative addition with cyclic alkanes

The ΔG_{rxn} (kcal/mol) of metallacycle formation (following schemes Figure 19 Figure 20) showing two trends: i) for a given transition metal catalyst, oxidative addition with cyclobutane (n = 2) is the most thermodynamically favorable, and reaction with cyclopentane (n = 3) is the least thermodynamically favorable, and ii) for a given cyclic ketone, the thermodynamic preference proceeds in the order Ir > Rh > Ni. The Gibbs free energies are with respect to the cyclic alkanes and transition metal complex (Ni(PPh$_3$)$_2$, Rh(dppm)Cl, or Ir(dppm)Cl). Note that for the reactions with Ni(PPh$_3$)$_2$, the resulting metallacycle product has a PPh$_3$ ligand dissociated from the metal (see Figure 19).

To understand these trends, ring strain energy calculations were performed on both the cyclic alkane reactants and the metallacycles (see section 2.1 for discussion of homodesmotic calculations). Figure 22 shows the results of these calculations. For a given transition metal catalyst, the five-membered metallacycle (n = 2) is the least strained, except in the case of the Ni-based metallacycles, where the six-membered metallacycle (n = 3) is slightly less strained. In all cases, Ni-based metallacycles are more strained than the corresponding Rh and Ir structures; this is in contrast to the ketone-based

metallacycles, where all systems of a given size had similar strain. These exceptions for Ni can be attributed to shorter Ni–C bond lengths (1.93 Å vs. 2.09 – 2.11 Å for Rh and Ir) and the accompanying bond angle considerations, and additionally to minor alkyl–Ni interactions stabilizing the acyclic structure used in the homodesmotic ring strain calculation. In all cases, the four-membered metallacycle is the most strained.
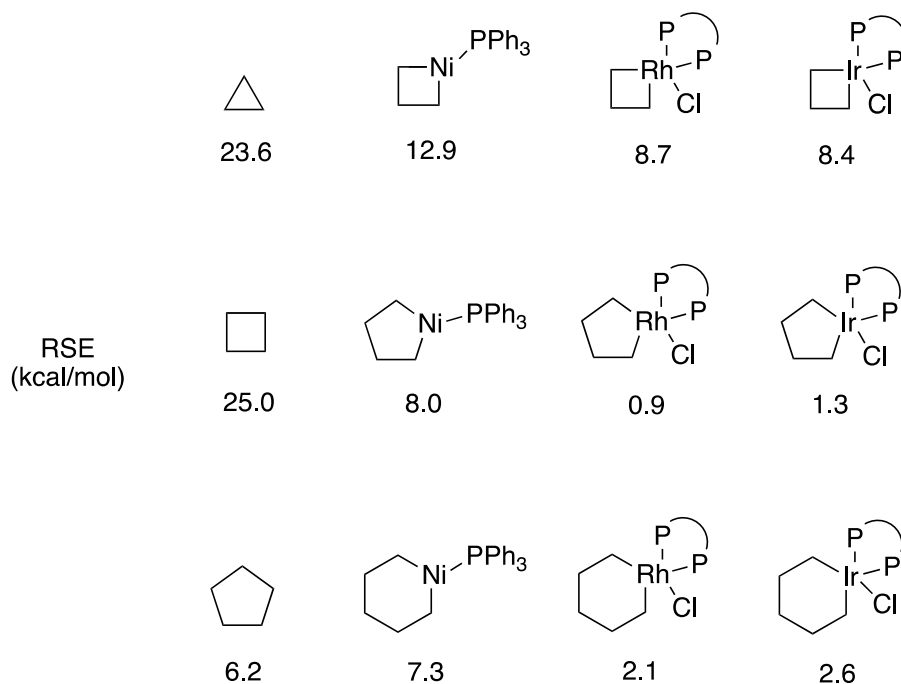
Figure 22: Ring strain energies of cyclic alkanes and metallacycles

All ring strain (kcal/mol) are calculated using a homodesmotic calculation (section 2.1). No significant interaction between these ligands and the metallacycle was present; see appendix Figure 40 for details.

However, when we turn our attention to the ring strain released through the reaction—the difference between the ring strain of the metallacycle and the cyclic alkane reactant—there is again a strong linear relationship with the ΔG_{rxn} (Figure 24). The strong linear relationship ($r^2 >= 0.98$) with a slope near 1 suggests that ring strain release is an independent driving force for the formation of these metallacycles. Note the ordering of the variously sized metallacycles is different than it was for the ketones; here oxidative addition to form the smallest metallacycles is intermediate in both ΔG_{rxn} and ring strain released. This different ordering is due to the drastically different ring strain of cyclopropane compared to cyclopropanone. The gaps between the linear fits for the different metals in Figure 14 (Ni ~= Rh > Ir) can be approximately accounted for by differences in C–M bond energies (Figure 25).
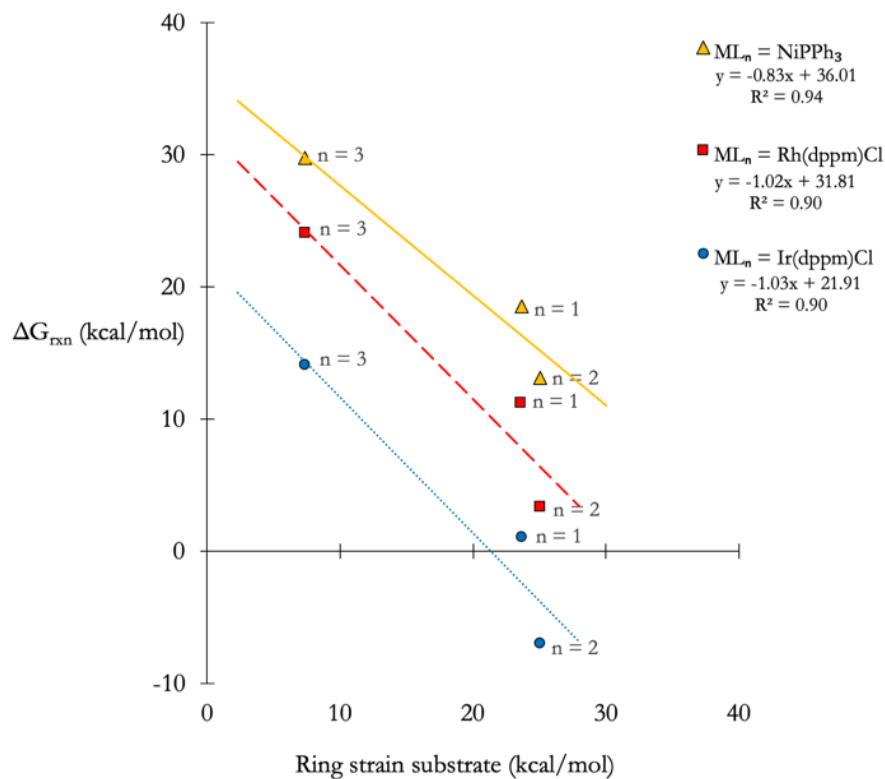
Figure 23: Ring strain substrate vs ΔG_{rxn} for oxidative addition of cyclic alkanes

The ring strain of the substrate (kcal/mol) vs. ΔG_{rxn} (kcal/mol) of the cyclic alkane oxidative addition. Again, 'n' corresponds to the size of the ketone reactant (see Schemes 2 and 3) with n = 1, 2, 3 corresponding to a three, four, and five membered ketone rings. The relationship is not as strong as that between ΔG_{rxn} and ring strain released (Figure 24).

28
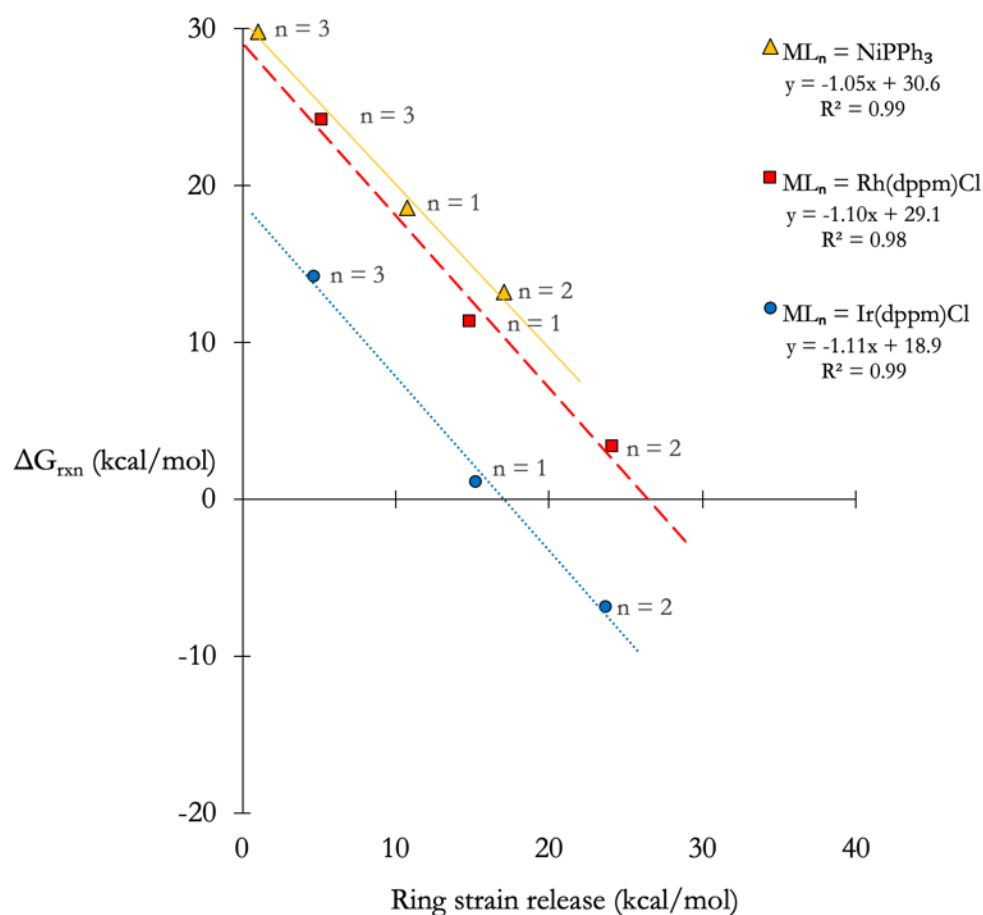
Figure 24: Ring strain release vs ΔG$_{rxn}$ for oxidative addition of cyclic alkanes

The ring strain release (kcal/mol) vs. ΔG$_{rxn}$ (kcal/mol) of the cyclic alkane oxidative addition. 'n' corresponds to the ring size of the alkane reactant (see Figure 19 and Figure 20) with n = 1, 2, 3 corresponding to a three-, four-, and five-membered alkanes. The strong linear relationship with a slope near 1 suggests ring strain release is an independent driving force of the reaction. Note the ordering of the differently sized metallacycles is different than it was for the ketones; here smallest metallacycles are intermediate in both ΔG$_{rxn}$ and ring strain released.
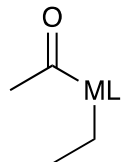
ML =	Ni(PPh₃)	Rh(dppm)Cl	Ir(dppm)Cl
Et—ML BDE (kcal/mol)	57.9	57.6	68.1

Figure 25: Metal-carbon bond energies

The carbon-metal bond dissociation energies (BDEs) for the three different metal complexes were examined. The BDEs mirror the Ni ~= Rh < Ir ordering observed in Figure 24. Note that there were no significant changes in these values for different alkyl chain lengths.

4.2 Kinetics of cyclic alkane oxidative addition

Transition states were located for all oxidative addition reactions detailed in Figure 26 and Figure 27. All activation Gibbs free energies are shown in Figure 28, which again shows that reactions with more strained reactants have a lower activation energy, and that given a cyclic alkane, the activation energy of the different transition metal complexes is similar to each other. As with oxidative addition of cyclic ketones (Chapter 3), the three transition metal catalysts appear to have a similar effect on $\Delta G^{\ddagger}$. All activation energies are higher than the corresponding reaction with cyclic ketones (compare to Figure 14), which agrees with the general lower reactivity of cycloaddition with cyclic alkanes.
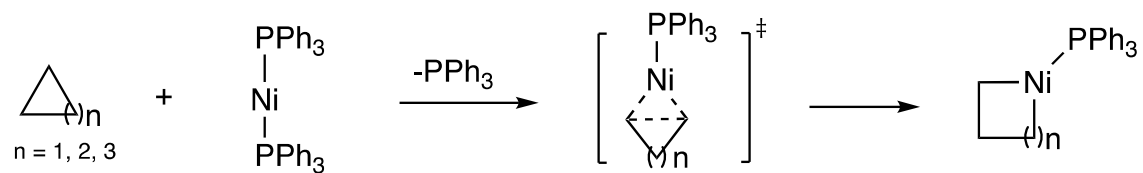
Figure 26: Transition state of oxidative addition of cyclic alkanes with a Ni(0) catalyst
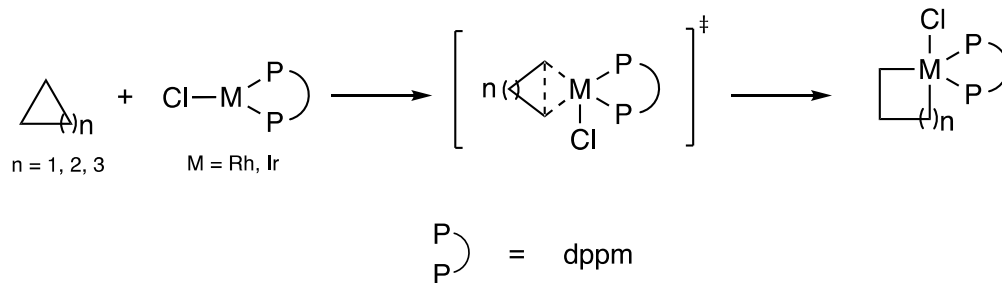
Figure 27: Transition state of oxidative addition of cyclic alkanes with Rh(I)- and Ir(I)-based catalysts
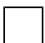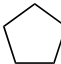
	NiPPh$_3$	RhCl(dppm)	IrCl(dppm)
△ n = 1	17.0	19.1	16.7
▢ n = 2	27.2	28.4	28.7
⬠ n = 3	37.5	40.3	39.6

Figure 28: ΔG‡ (kcal/mol) of oxidative addition of cyclic alkanes

The $\Delta G^{‡}$ (kcal/mol) of the oxidative addition reactions (following Figure 26 and Figure 27) showing that for a given transition metal catalyst, the expansion of the smaller cyclic alkanes is more kinetically favorable. Given a cyclic alkane, oxidative addition with the three transition metal catalysts all have similar activation free energies. Compared to the corresponding activation energies for the oxidative addition of cyclic ketones (Figure 14), the cyclic alkanes are less reactive.

When the relationship between ΔG_{rxn} vs $\Delta G^{‡}$ is plotted, a major difference between the ketone- and alkane-based oxidative additions becomes apparent: where the oxidative addition of cyclic ketones showed a linear relationship between ΔG_{rxn} vs $\Delta G^{‡}$ (Figure 15), this is not the case for the oxidative addition of cyclic alkanes (Figure 29). This is likely due to the unusual 'banana' bonding of cyclopropane (n = 1), which stabilizes the transition state of these reactions.[74] Additionally, while cyclopropane and cyclobutane have comparable ring strain, oxidative addition with cyclopropane is

less exergonic because the resulting four-membered metallacycles are more strained than the five-membered metallacycles that result from oxidative addition with cyclobutane.

The irregularity of the oxidative additions with cyclopropane is apparent also from an examination of the transition states (those for Rh shown in Figure 30), where we see an exception to the general trend of earlier transition states for more strained reactants. The TS for the oxidative addition of cyclopropane exhibits an unusually close distance for the forming C–M bonds, likely due to cyclopropane's unusually accessible C–C σ bonds.

As can be anticipated given the foregoing discussion, $\Delta G^{\ddagger}$ is poorly correlated with both ring strain release (Figure 32) and the ring strain of the starting reagents (Figure 31). The magnitude of the RSR shows that the RSR of the cyclic alkanes is generally lower than that of the cyclic ketones (compare Figure 18), but not enough to wholly account for their overall lower reactivity. Again, the question of how much strain energy is released by the transition state was ultimately set aside due to difficulties quantifying TS strain energy in a way that is consistent and meaningful across the different systems.
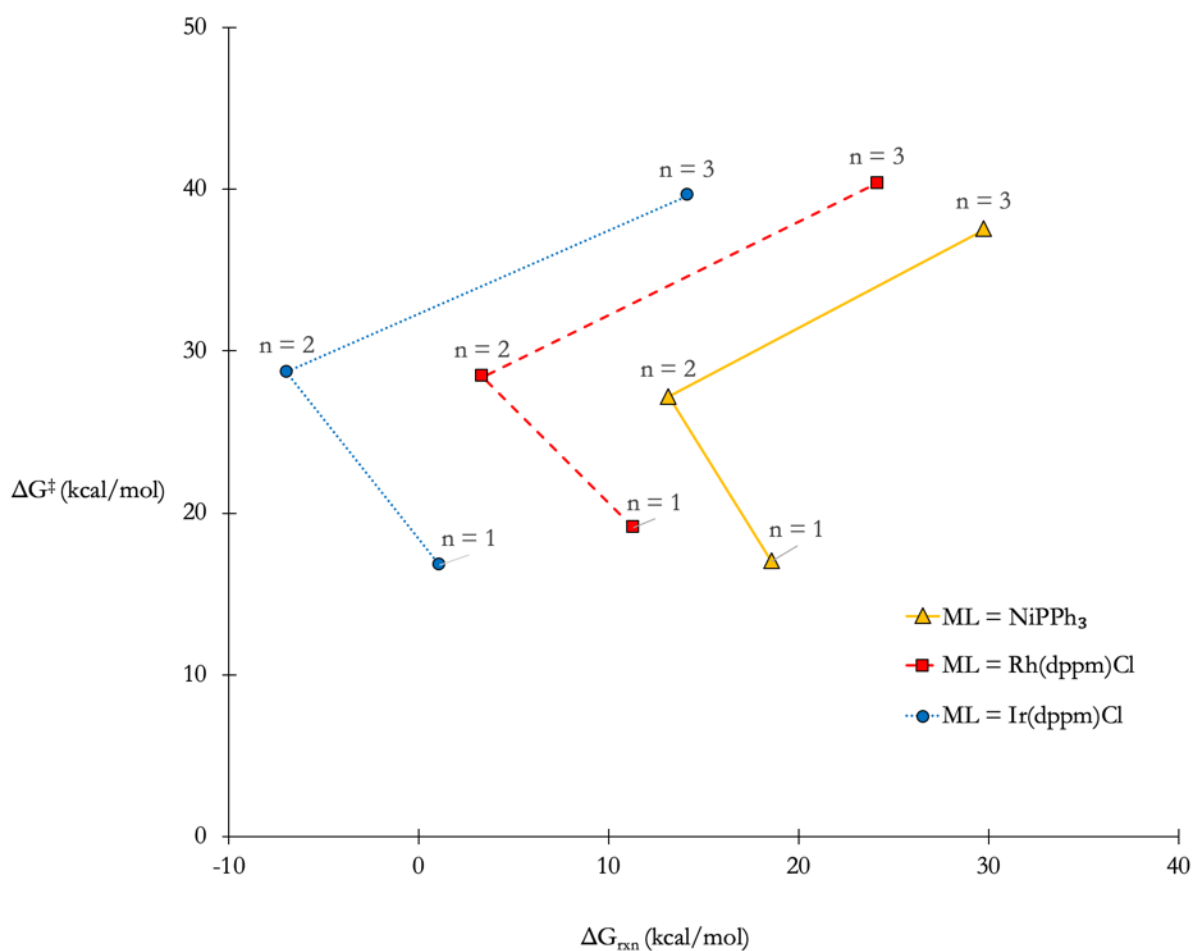
Figure 29: ΔG_{rxn} vs $\Delta G^{\ddagger}$ of oxidative addition of cyclic alkanes

This non-linearity is in sharp contrast to the corresponding figure for the oxidative addition of cyclic ketones (Figure 15). The higher reactivity of cyclopropane compared to cyclobutane despite the smaller amount of ring strain release is likely due to the unusual 'banana' bonding of cyclopropane, lowering the energy of the transition states with these substrates.
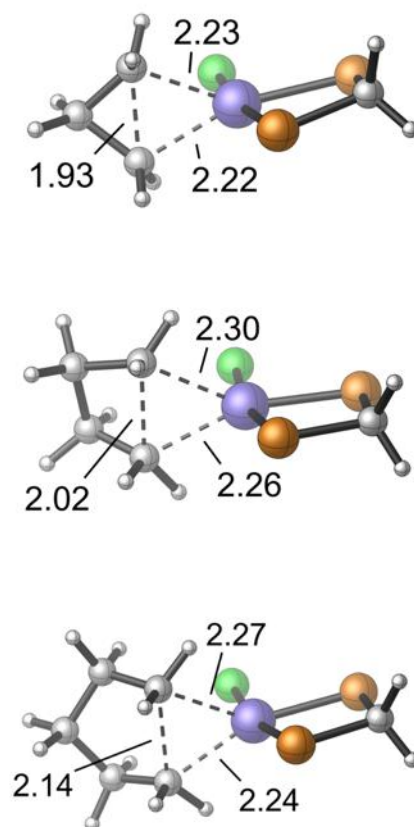
Figure 30: Transition states of the oxidative addition of cyclic alkanes using and Rh(I) catalyst

These transition states for the oxidative addition of cyclic alkanes are less straightforward than those of cyclic ketones. While the formation of the 5- and 6-membered metallacycles shows a later transition state for the reaction with the larger and more stable cyclopentane vs cyclobutane, the reaction with cyclopropane is irregular in the shorter length of the forming C–M bonds. This is likely due to cyclopropane's unusually accessible C–C σ bonds.
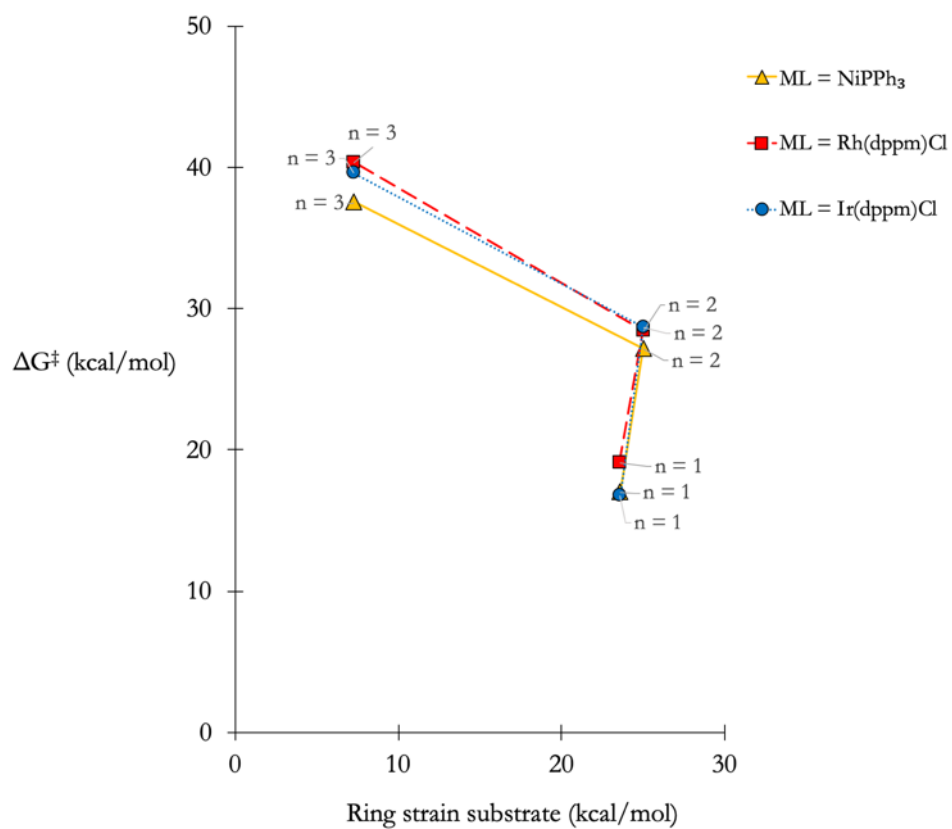
Figure 31: Ring strain substrate vs $\Delta G^{\ddagger}$ for the oxidative addition of cyclic alkanes

The transition state energies are also very poorly correlated with the ring strain of the cyclic alkane reagents. Again, this is likely due to the exceptional nature of cyclopropane.
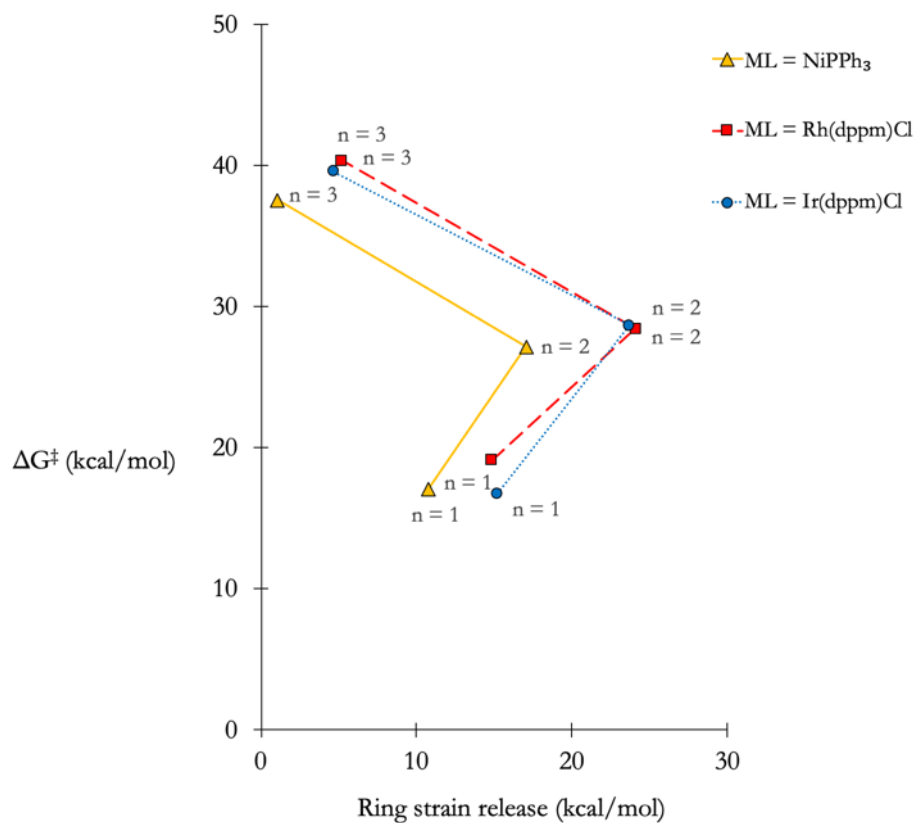
Figure 32: Ring strain release vs $\Delta G^{\ddagger}$ for the oxidative addition of cyclic alkanes

The transition state energies are very poorly correlated with ring strain release, unlike the energies and rates of oxidative addition with cyclic ketones. This is likely due to the exceptional nature of cyclopropane. Compared to these values of corresponding reactions with cyclic ketones (Figure 18), there is generally less RSR for the cyclic alkanes.

5.0 Conclusion

The five-membered metallacycles explored in this work possess less ring strain than their four- and six-membered counterparts—a fact that can be accounted for primarily by bond angle considerations—but the reaction energies of their formation via oxidative addition must be understood in conjunction with the ring strain of the cyclic reagents. The reaction energies of the oxidative addition of both cyclic ketones and cyclic alkanes are driven primarily by ring strain release (RSR), i.e. the ring strain energy difference between the cyclic starting material and the metallacycle formed after the oxidative addition. There are strong linear relationships between ΔG_{rxn} and RSR for all six series of varying ring sizes explored in this work. Notably, this holds true despite that oxidative addition of cyclic ketones show a thermodynamic preference for smaller ring sizes, while the oxidative addition of cyclic alkanes show a thermodynamic preference for cyclobutane over cyclopropane. While there is a strong correlation between ΔG_{rxn} and the ring strain of the cyclic ketone substrates, this correlation is slightly weaker in the case of the cyclic alkanes. Additionally, the reaction energies with cyclic ketones are also strongly influenced by the identity of the metal center. Different metals have varying degrees of backdonation from the metal to C=O π^*, which accounts for the trend in ΔG_{rxn} (and carbon-metal bond strength) of the metals: Ir > Rh > Ni. On the other hand, backbonding is not expected to play a significant role in the reactivity of the cyclic alkanes due to the absence of a suitable orbital for accepting electron density from the metal centers.

The activation Gibbs free energies of oxidative addition with cyclic ketones follow a similar trend, where $\Delta G^{\ddagger}$ is well correlated with both the ring strain of the substrates as well as RSR. However, backdonation from the metals appears to have no significant effect on $\Delta G^{\ddagger}$, even in the case of

oxidative addition with cyclic ketones, which is likely due to the greater distance between the relevant orbitals in the transition state when compared to the resulting metallacycles. In fact, nor does anything else about the identity of the metal center appears to significantly impact $\Delta G^{\ddagger}$: given a cyclic reagent, the activation energies of its oxidative addition with any of the metal complexes explored in this work are all comparable. Trends in the $\Delta G^{\ddagger}$ of oxidative addition with cyclic alkanes are complicated by the exceptional reactivity of the cyclopropane substrate: while barely more strained than cyclobutane, the reactivity of cyclopropane is not only promoted by ring strain, but also its highly accessible 'banana'-like σ bonds. This behavior is reflected in the bond lengths of the oxidative addition transition states involving cyclopropane, where the breaking C-C bond *and* the forming C-M bonds are shorter than corresponding reactions with cyclobutane and cyclopentane. In all cases, the $\Delta G^{\ddagger}$ is much less sensitive to the different metal complexes than ΔG, suggesting that the kinetics are primarily controlled by the properties of the substrate, and that all three metal complexes may be capable of promoting oxidative addition.

These results offer several points that can be used to guide experimental work in this area. First, when determining whether oxidative addition reactions with cyclic reagents are thermodynamically feasible, RSR is a more useful metric to focus on than the strain of the starting reagent or of the resulting metallacycle in isolation. What might appear to be deviations to simple trends in the thermodynamics can be accounted for by RSR release considerations: cleaving the three-membered ring in cyclopropane is less thermodynamically favorable than cleaving cyclobutane because, while both reagents have similar ring strain, the four-membered-metallacycles still have considerable strain, whereas the five-membered metallacycles possess very little strain (even less than their six-membered counterparts). Conversely, cleaving the three-membered cyclopropanone is more thermodynamically favorable than cleaving cyclobutanone because, while the resulting four-membered metallacycles are

more strained than the five-membered counterparts, cyclopropanone is considerably more strained than cyclobutanone.

Second, oxidative addition is kinetically feasible for all studied reactions, even with relatively stable cyclic reagents. Furthermore, as noted above, the activation Gibbs free energies are largely insensitive to the identity of the metal center, suggesting that this feasibility will hold more generally. However, many of these reactions are endergonic, which may lead to a higher overall barrier for subsequent functionalization steps, and thereby limit their utility for such purposes. Therefore, both kinetics and thermodynamics of the C–C bond cleavage step should be considered when utilizing these reactions in synthesis. On the other hand, oxidative addition of Ir- and Rh-based catalysts with cyclic ketones is quite exergonic, due in part to stronger carbonyl backbonding, and thus make them privileged catalysts for ketone C–C bond activation reactions.
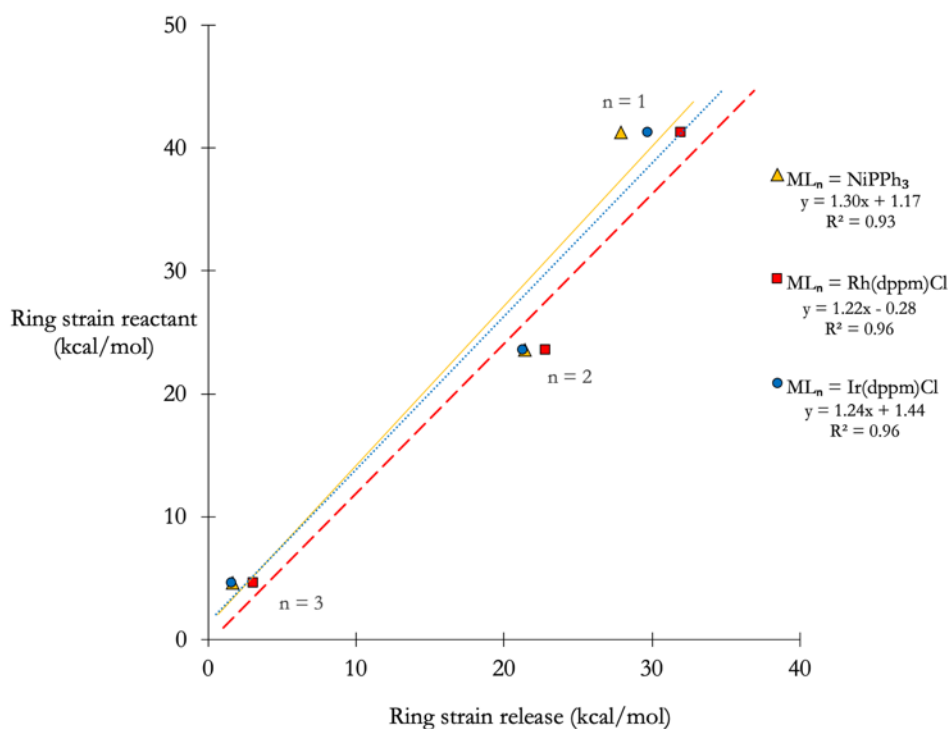
Figure 33: Ring strain release vs ring strain reactant for the oxidative addition of cyclic ketones

The approximately linear relationship between ring strain release and ring strain of the reactant, coupled with both being correlated with correlated with ΔG_{rxn} (see Figure 10 and Figure 9) make it difficult to ascertain which is driving the thermodynamics of these reactions. However, for both the cyclic ketone and cyclic alkane reactions, the correlation is strongest between ΔG_{rxn} and ring strain release, which suggests it is the release of ring strain that primarily drives the thermodynamics.

30

n = 1
n = 2

△ ML_n = NiPPh₃

$y = 1.16x + 7.53$
$R^2 = 0.89$

n = 2
n = 1
n = 1
n = 2

20

Ring strain reactant
(kcal/mol)

■ ML_n = Rh(dppm)Cl

$y = 0.94x + 4.75$
$R^2 = 0.82$

● ML_n = Ir(dppm)Cl

$y = 0.95x + 4.77$
$R^2 = 0.85$

10

n = 3
n = 3
n = 3

0

0   10   20   30   40

Ring strain release (kcal/mol)
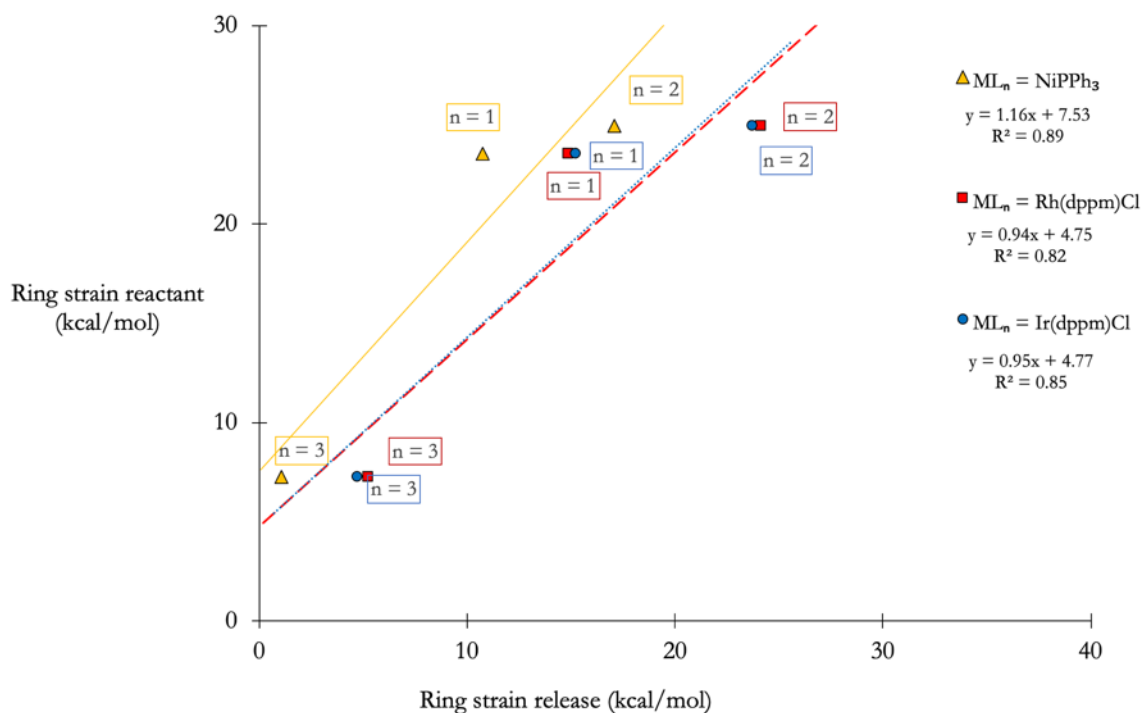
Figure 34: Ring strain release vs ring strain reactant for the oxidative addition of cyclic alkanes

The approximately linear relationship between ring strain release and ring strain of the reactant, coupled with both being correlated with correlated with ΔG_{rxn} (see Figure 10 and Figure 9) make it difficult to ascertain which is driving the thermodynamics of these reactions. However, for both the cyclic ketone and cyclic alkane reactions, the correlation is strongest between ΔG_{rxn} and ring strain release, which suggests it is the release of ring strain that primarily drives the thermodynamics.
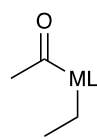
	ML = Ni(PPh$_3$)	Rh(dppm)Cl	Ir(dppm)Cl
NPA charge on O (e$^-$)	-0.561	-0.564	-0.587
C=O frequency (cm^{-1})	1681	1770	1745

Figure 35: Backbonding as per NPA charge and C=O frequency in acyclic structure

These metrics do not provide significant support for the idea that Ir engages in the most backbonding with C=O, followed by Rh and lastly Ni. While the NPA charge on oxygen follows this trend, the magnitude of the different values is quite small. The C=O frequency does not follow the same trend, perhaps due to minor additional ligand effects (though it is difficult to make this case given the amount of space available to the ligands; see appendix Figure 36).
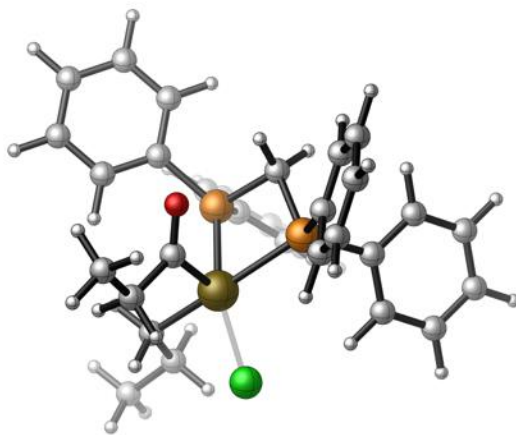
Figure 36: Minimal ligand-carboxyl interaction

Rh acyclic complex is shown. With ample space separating the carboxy group and the other ligands, it is unclear why the C=O vibrational frequency does not follow the trend expected based on backbonding considerations (Figure 35).

43
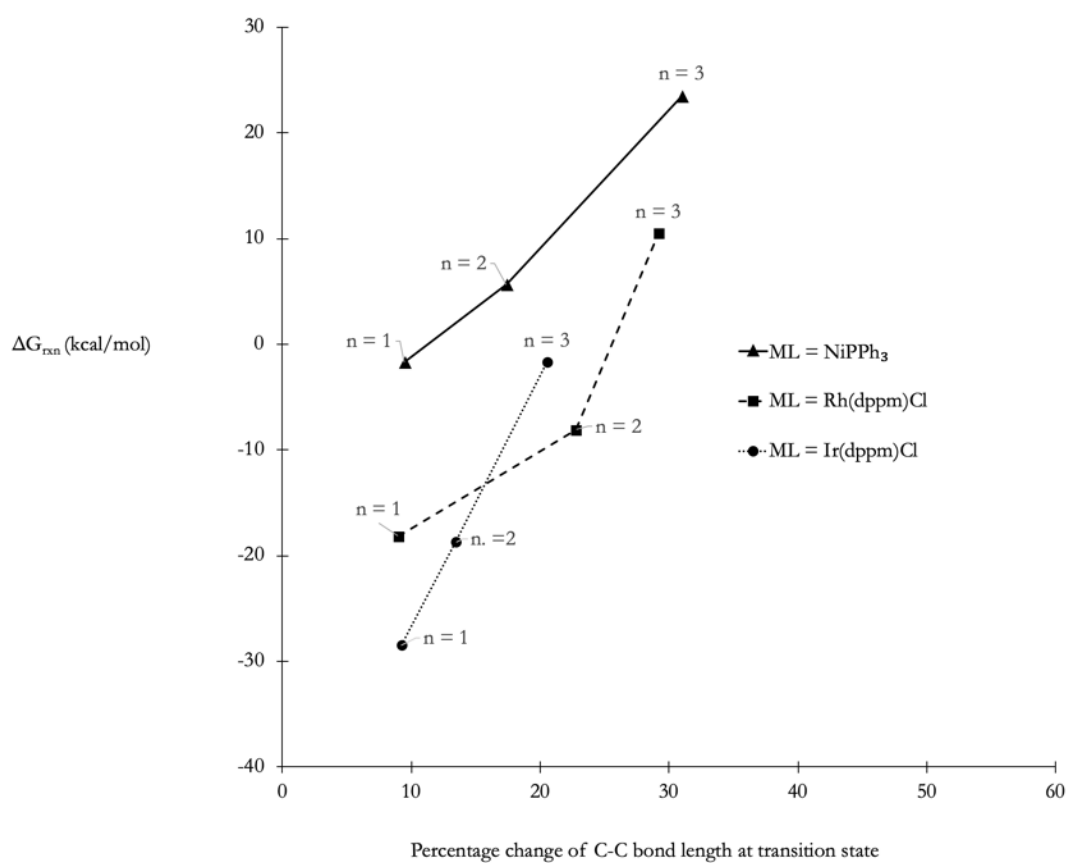
Figure 37: Percentage change of C-C bond length at TS for the oxidative addition of cyclic ketones

The linearity of these series suggests that the oxidative addition of the three cyclic ketones follow same mechanism (and follows the Hammond postulate).
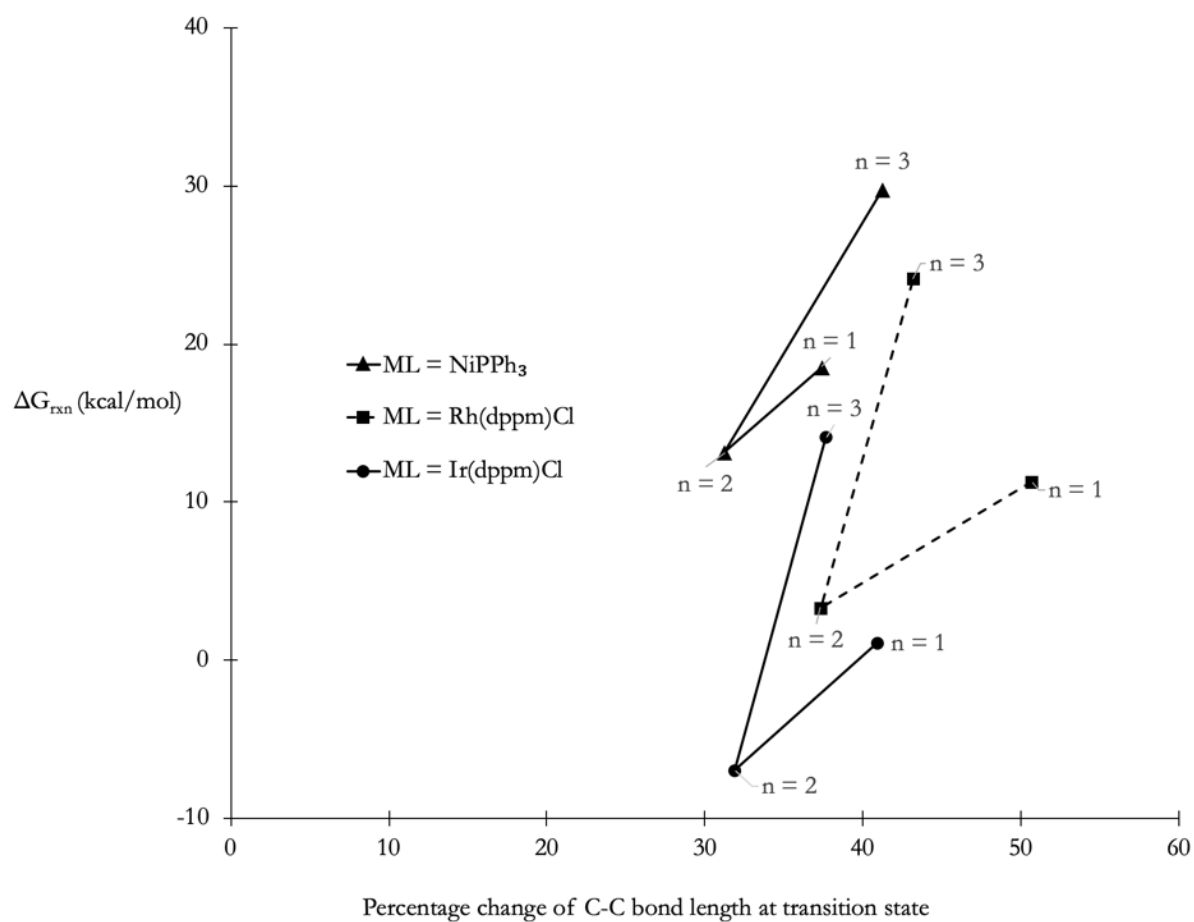
Figure 38: Percentage change of C-C bond length at TS for the oxidative addition of cyclic alkanes

The non-linearity of these series supports the idea that the oxidative addition of the examined cyclic alkanes do not follow the same mechanism (and do not follow the Hammond postulate). This is likely due to the exceptional nature of cyclopropane, as discussed in the body of this work.
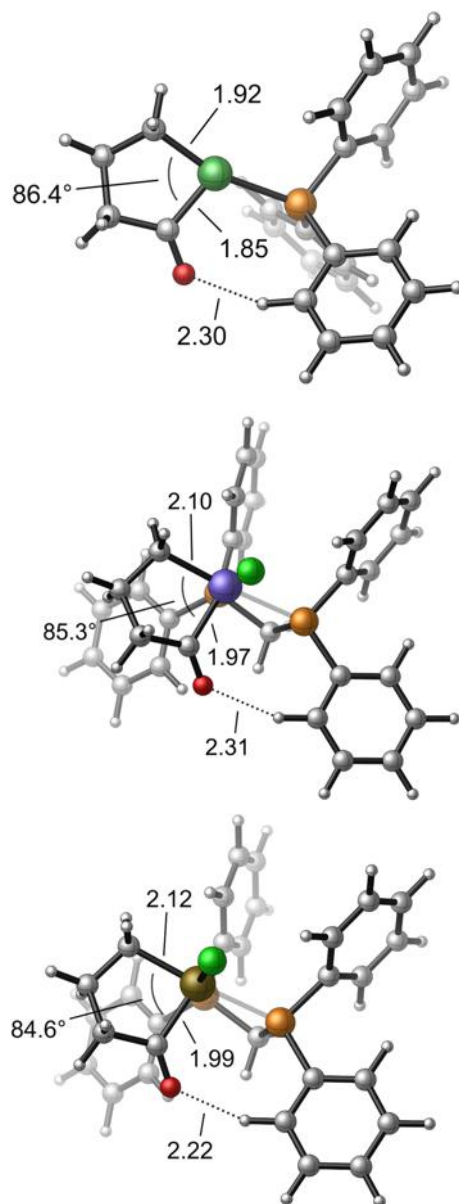
Figure 39: C-M-C bond angles and C-M bond lengths for the oxidative addition of cyclic ketones

Five-membered metallacycles for Ni (top), Rh (middle), and Ir (bottom) complexes as detailed in Figure 8. As the C-M-C bond angles decreases Ni > Rh > Ir, the C-M bond lengths increase. As all systems have very little ring strain, this may merely be due to the size of the metals. The distance between the carboxyl oxygen and nearest aryl group shows there is relatively little interaction between the metallacycle and the rest of the ligands.

46
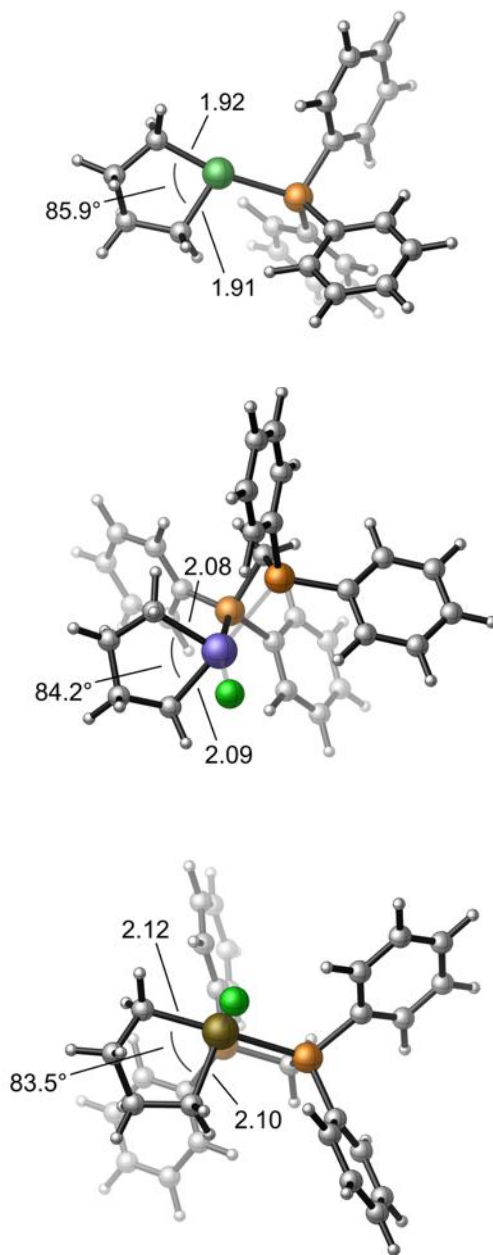
Figure 40: C-M-C bond angles and C-M bond lengths for the oxidative addition of cyclic alkanes

Five-membered metallacycles for Ni (top), Rh (middle), and Ir (bottom) complexes as detailed in Figure 22. As the C-M-C bond angles decreases Ni > Rh > Ir, the C-M bond lengths increase. While this is consistent with the Ni metallacycle being the most strained, the Rh and Ir systems both have very little ring strain energy; the comparison of their angle and bond lengths is likely merely a reflection of the size of the metals.

Bibliography

1.	Dong, G. *C-C Bond Activation*. (Springer Berlin Heidelberg, 2014). doi:10.1007/978-3-642-55055-3

2.	Jones, W. D. Mechanistic studies of transition metal-mediated c–c bond activation. *Top. Curr. Chem.* **346**, 1–32 (2014).

3.	Jun, C. H. & Park, J. W. Metal–organic cooperative catalysis in C–C bond activation. *Top. Curr. Chem.* **346**, 59–84 (2014).

4.	Gao, Y., Fu, X. F. & Yu, Z. X. Transition metal-catalyzed cycloadditions of cyclopropanes for the synthesis of carbocycles: C–C activation in cyclopropanes. *Top. Curr. Chem.* **346**, 195–232 (2014).

5.	Xu, T., Dermenc, A. & Dong, G. Transition metal-catalyzed c–c bond activation of four-membered cyclic ketones. *Top. Curr. Chem.* **346**, 233–258 (2014).

6.	Chen, P., Billett, B. A., Tsukamoto, T. & Dong, G. "Cut and Sew" Transformations via Transition-Metal-Catalyzed Carbon–Carbon Bond Activation. *ACS Catal.* **7**, 1340–1360 (2017).

7.	Rubin, M., Rubina, M. & Gevorgyan, V. Transition metal chemistry of cyclopropenes and cyclopropanes. *Chem. Rev.* **107**, 3117–3179 (2007).

8.	Souillart, L. & Cramer, N. Catalytic C–C Bond Activations via Oxidative Addition to Transition Metals. *Chem. Rev.* **115**, 9410–9464 (2015).

9.	Butenschön, H. Seven-membered rings by cyclization at transition metals: [4+3], [3+2+2], [5+2]. *Angew. Chemie - Int. Ed.* **47**, 5287–5290 (2008).

10.	Ruhland, K. Transition-Metal-Mediated Cleavage and Activation of C-C Single Bonds. *European J. Org. Chem.* **2012**, 2683–2706 (2012).

11.	Crabtree, R. H., Dion, R. P., Gibboni, D. J., McGrath, D. V. & Holt, E. M. C–C Bond Cleavage in Hydrocarbons by Iridium Complexes. *J. Am. Chem. Soc.* **108**, 7222–7227 (1986).

12.	Saito, S., Komagawa, S., Azumaya, I. & Masuda, M. Nickel-catalyzed intermolecular [3 + 2 + 2] cocyclization of ethyl cyclopropylideneacetate and alkynes. Synthesis of seven-membered carbocycles. *J. Org. Chem.* **72**, 9114–9120 (2007).

13.	Shimizu, I., Ohashi, Y. & Tsuji, J. Palladium-catalyzed [3 + 2] cycloaddition reaction of vinylcyclopropanes with α,β-unsaturated esters or ketones. *Tetrahedron Lett.* **26**, 3825–3828 (1985).

14.   Trost, B. M. & Chan, D. M. T. Palladium-Mediated Cycloaddition Approach to Cyclopentanoids. Introduction and Initial Studies. *J. Am. Chem. Soc.* **105**, 2315–2325 (1983).

15.   Kondo, T. Ruthenium- and Rhodium-Catalyzed Strain-Driven Cleavage and Reconstruction of the C-C Bond. *European J. Org. Chem.* **2016**, 1232–1242 (2016).

16.   Murakami, M., Amii, H., Shigeto, K. & Ito, Y. Breaking of the C-C bond of cyclobutanones by rhodium(I) and its extension to catalytic synthetic reactions. *J. Am. Chem. Soc.* **118**, 8285–8290 (1996).

17.   Nishimura, T., Araki, H., Maeda, Y. & Uemura, S. Palladium-catalyzed oxidative alkynylation of alkenes via C-C bond cleavage under oxygen atmosphere. *Org. Lett.* **5**, 2997–2999 (2003).

18.   William Suggs, J. & Jun, C. H. Directed Cleavage of Carbon-Carbon Bonds by Transition Metals: The α-Bonds of Ketones. *J. Am. Chem. Soc.* **106**, 3054–3056 (1984).

19.   Ritleng, V., Sirlin, C. & Pfeffer, M. Ru-, Rh-, and Pd-catalyzed C-C bond formation involving C-H activation and addition on unsaturated substrates: Reactions and mechanistic aspects. *Chem. Rev.* **102**, 1731–1769 (2002).

20.   Matsuda, T., Shigeno, M. & Murakami, M. Asymmetric synthesis of 3,4-dihydrocoumarins by rhodium-catalyzed reaction of 3-(2-hydroxyphenyl)cyclobutanones. *J. Am. Chem. Soc.* **129**, 12086–12087 (2007).

21.   Nogi, K. & Yorimitsu, H. Carbon–Carbon Bond Cleavage at Allylic Positions: Retro-allylation and Deallylation. *Chem. Rev.* **121**, 345–364 (2020).

22.   Huffman, M. A., Liebeskind, L. S. & Pennington, W. T. Reaction of cyclobutenones with low-valent metal reagents to form .eta.4- and .eta.2-vinylketene complexes. Reaction of .eta.4-vinylketene complexes with alkynes to form phenols. *Organometallics* **11**, 255–266 (1992).

23.   Fumagalli, G., Stanton, S. & Bower, J. F. Recent Methodologies That Exploit C–C Single-Bond Cleavage of Strained Ring Systems by Transition Metal Complexes. *Chem. Rev.* **117**, 9404–9432 (2017).

24.   Chen, P. H., Sieber, J., Senanayake, C. H. & Dong, G. Rh-catalyzed reagent-free ring expansion of cyclobutenones and benzocyclobutenones. *Chem. Sci.* **6**, 5440–5445 (2015).

25.   Xu, T. & Dong, G. Rhodium-Catalyzed Regioselective Carboacylation of Olefins: A C-C Bond Activation Approach for Accessing Fused-Ring Systems. *Angew. Chemie Int. Ed.* **51**, 7567–7571 (2012).

26.   Xia, Y. & Dong, G. Temporary or removable directing groups enable activation of unstrained C–C bonds. doi:10.1038/s41570-020-0218-8

27.   Lee, C., Yang, W. & Parr, R. G. Development of the Colle-Salvetti correlation-energy formula into a functional of the electron density. *Phys. Rev. B* **37**, 785 (1988).

28.   Becke, A. D. Density-functional exchange-energy approximation with correct asymptotic

behavior. *Phys. Rev. A* **38**, 3098 (1988).

29. Stephens, P. J., Devlin, F. J., Chabalowski, C. F. & Frisch, M. J. Ab Initio Calculation of Vibrational Absorption and Circular Dichroism Spectra Using Density Functional Force Fields. *J. Phys. Chem.* **98**, 11623–11627 (2002).

30. Hay, P. J. & Wadt, W. R. Ab initio effective core potentials for molecular calculations. Potentials for K to Au including the outermost core orbitale. *J. Chem. Phys.* **82**, 299–310 (1985).

31. Wadt, W. R. & Hay, P. J. Ab initio effective core potentials for molecular calculations. Potentials for main group elements Na to Bi. *J. Chem. Phys.* **82**, 284–298 (1985).

32. Hay, P. J. & Wadt, W. R. Ab initio effective core potentials for molecular calculations. Potentials for the transition metal atoms Sc to Hg. *J. Chem. Phys.* **82**, 270–283 (1985).

33. Hehre, W. J., Ditchfield, K. & Pople, J. A. Self-consistent molecular orbital methods. XII. Further extensions of gaussian-type basis sets for use in molecular orbital studies of organic molecules. *J. Chem. Phys.* **56**, 2257–2261 (1972).

34. Ditchfield, R., Hehre, W. J. & Pople, J. A. Self-consistent molecular-orbital methods. IX. An extended gaussian-type basis for molecular-orbital studies of organic molecules. *J. Chem. Phys.* **54**, 720–723 (1971).

35. Hariharan, P. C. & Pople, J. A. Accuracy of AHn equilibrium geometries by single determinant molecular orbital theory. *Mol. Phys.* **27**, 209–214 (1974).

36. Hariharan, P. C. & Pople, J. A. The influence of polarization functions on molecular orbital hydrogenation energies. *Theor. Chim. Acta* **28**, 213–222 (1973).

37. Gordon, M. S. The isomers of silacyclopropane. *Chem. Phys. Lett.* **76**, 163–168 (1980).

38. Francl, M. M. *et al.* Self-consistent molecular orbital methods. XXIII. A polarization-type basis set for second-row elements. *J. Chem. Phys.* **77**, 3654–3665 (1982).

39. Binning, R. C. & Curtiss, L. A. Compact contracted basis sets for third-row atoms: Ga–Kr. *J. Comput. Chem.* **11**, 1206–1216 (1990).

40. Zhao, Y., Truhlar, D. G., Zhao, Y. & Truhlar, · D G. The M06 suite of density functionals for main group thermochemistry, thermochemical kinetics, noncovalent interactions, excited states, and transition elements: two new functionals and systematic testing of four M06-class functionals and 12 other functionals. *Theor. Chem. Accounts 2007 1201* **120**, 215–241 (2007).

41. Blaudeau, J. P., McGrath, M. P., Curtiss, L. A. & Radom, L. Extension of Gaussian-2 (G2) theory to molecules containing third-row atoms K and Ca. *J. Chem. Phys.* **107**, 5016–5021 (1997).

42. Rassolov, V. A., Ratner, M. A., Pople, J. A., Redfern, P. C. & Curtiss, L. A. 6-31G* basis set for third-row atoms. *J. Comput. Chem.* **22**, 976–984 (2001).

43. Küchle, W., Dolg, M., Stoll, H. & Preuss, H. Energy-adjusted pseudopotentials for the

actinides. Parameter sets and test calculations for thorium and thorium monoxide. *J. Chem. Phys.* **100**, 7535–7542 (1994).

44. Schwerdtfeger, P., Dolg, M., Schwarz, W. H. E., Bowmaker, G. A. & Boyd, P. D. W. Relativistic effects in gold chemistry. I. Diatomic gold compounds. *J. Chem. Phys.* **91**, 1762–1774 (1989).

45. Dolg, M., Stoll, H., Savin, A. & Preuss, H. Energy-adjusted pseudopotentials for the rare earth elements. *Theor. Chim. Acta* **75**, 173–194 (1989).

46. Andrae, D., Häußermann, U., Dolg, M., Stoll, H. & Preuß, H. Energy-adjusted ab initio pseudopotentials for the second and third row transition elements. *Theor. Chim. Acta* **77**, 123–141 (1990).

47. Dolg, M., Fulde, P., Küchle, W., Neumann, C. S. & Stoll, H. Ground state calculations of di-π-cyclooctatetraene cerium. *J. Chem. Phys.* **94**, 3011–3017 (1991).

48. Kaupp, M., Schleyer, P. V. R., Stoll, H. & Preuss, H. Pseudopotential approaches to Ca, Sr, and Ba hydrides. Why are some alkaline earth MX2 compounds bent? *J. Chem. Phys.* **94**, 1360–1366 (1991).

49. Rassolov, V. A., Pople, J. A., Ratner, M. A. & Windus, T. L. 6-31G* basis set for atoms K through Zn. *J. Chem. Phys.* **109**, 1223–1229 (1998).

50. Fuentealba, P., Von Szentpaly, L., Preuss, H. & Stoll, H. Pseudopotential calculations for alkaline-earth atoms. *J. Phys. B At. Mol. Phys.* **18**, 1287–1296 (1985).

51. Stoll, H. *et al.* Cu and Ag as one-valence-electron atoms: CI results and quadrupole corrections for Cu2, Ag2, CuH, and AgH. *J. Chem. Phys.* **81**, 2732–2736 (1984).

52. Fuentealba, P., Stoll, H., Von Szentpaly, L., Schwerdtfeger, P. & Preuss, H. On the reliability of semi-empirical pseudopotentials: Simulation of hartree-fock and dirac-fock results. *J. Phys. B At. Mol. Phys.* **16**, (1983).

53. von Szentpály, L., Fuentealba, P., Preuss, H. & Stoll, H. Pseudopotential calculations on Rb+2, Cs+2, RbH+, CsH+ and the mixed alkali dimer ions. *Chem. Phys. Lett.* **93**, 555–559 (1982).

54. Fuentealba, P., Preuss, H., Stoll, H. & Von Szentpály, L. A proper account of core-polarization with pseudopotentials: single valence-electron alkali compounds. *Chem. Phys. Lett.* **89**, 418–422 (1982).

55. Dolg, M., Wedig, U., Stoll, H. & Preuss, H. Energy-adjusted ab initio pseudopotentials for the first row transition elements. *J. Chem. Phys.* **86**, 866–872 (1986).

56. Igel-Mann, G., Stoll, H. & Preuss, H. Pseudopotentials for main group elements (IIIa through VIIa). *Mol. Phys.* **65**, 1321–1328 (1988).

57. McLean, A. D. & Chandler, G. S. Contracted Gaussian basis sets for molecular calculations. I. Second row atoms, Z=11-18. *J. Chem. Phys.* **72**, 5639–5648 (1980).

58.   Krishnan, R., Binkley, J. S., Seeger, R. & Pople, J. A. Self-consistent molecular orbital methods. XX. A basis set for correlated wave functions. *J. Chem. Phys.* **72**, 650–654 (1980).

59.   Barone, V. & Cossi, M. Quantum Calculation of Molecular Energies and Energy Gradients in Solution by a Conductor Solvent Model. *J. Phys. Chem. A* **102**, 1995–2001 (1998).

60.   Marenich, A. V., Cramer, C. J. & Truhlar, D. G. Universal solvation model based on solute electron density and on a continuum model of the solvent defined by the bulk dielectric constant and atomic surface tensions. *J. Phys. Chem. B* **113**, 6378–6396 (2009).

61.   Ochterski, J. Thermochemistry in Gaussian | Gaussian.com. Available at: https://gaussian.com/thermo/. (Accessed: 15th March 2022)

62.   Frisch, M. J., Trucks, G. W., Schlegel, H. B., Scuseria, G. E., Robb, M. A., Cheeseman, J. R., Scalmani, G., Barone, V., Petersson, G. A., Nakatsuji, H., Li, X., Caricato, M., Marenich, A. V., Bloino, J., Janesko, B. G., Gomperts, R., Mennucci, B., Hratch, D. J. Gaussian 16. (2016).

63.   Glendening *et al.* NBO 6.0: Natural Bond Orbital Analysis program. (2013).

64.   Wiberg, K. B. The Concept of Strain in Organic Chemistry. *Angew. Chemie Int. Ed. English* **25**, 312–322 (1986).

65.   George, P., Trachtman, M., Bock, C. W. & Brett, A. M. Homodesmotic reactions for the assessment of stabilization energies in benzenoid and other conjugated cyclic hydrocarbons. *J. Chem. Soc. Perkin Trans. 2* 1222–1227 (1976). doi:10.1039/P29760001222

66.   George, P., Trachtman, M., Bock, C. W. & Brett, A. M. An alternative approach to the problem of assessing stabilization energies in cyclic conjugated hydrocarbons. *Theor. Chim. Acta* **38**, 121–129 (1975).

67.   Hehre, W. J., Ditchfield, R., Radom, L. & Pople, J. A. Molecular Orbital Theory of the Electronic Structure of Organic Compounds. V. Molecular Theory of Bond Separation. *J. Am. Chem. Soc.* **92**, 4796–4801 (1970).

68.   Wheeler, S. E., Houk, K. N., Schleyer, P. v. R. & Allen, W. D. A Hierarchy of Homodesmotic Reactions for Thermochemistry. *J. Am. Chem. Soc.* **131**, 2547–2560 (2009).

69.   Wodrich, M. D. *et al.* The Concept of Protobranching and Its Many Paradigm Shifting Implications for Energy Evaluations. *Chem. - A Eur. J.* **13**, 7731–7744 (2007).

70.   Bachrach, S. M. The group equivalent reaction: An improved method for determining ring strain energy. *J. Chem. Educ.* **67**, 907–908 (1990).

71.   Fu, Y., Zerull, E. E., Schomaker, J. M. & Liu, P. Origins of Catalyst-Controlled Selectivity in Ag-Catalyzed Regiodivergent C-H Amination. *J. Am. Chem. Soc.* **144**, 2735–2746 (2022).

72.   De Lio, A. M., Durfey, B. L. & Gilbert, T. M. Estimating Ring Strain Energies of Highly Substituted Cyclohexanes with the Semi-homodesmotic Approach: Why Substantial Ring Strain Exists for Nominally Tetrahedral Ring Carbon Atoms. *J. Org. Chem.* **80**, 10234–10243

(2015).

73. Xia, Y., Lu, G., Liu, P. & Dong, G. Catalytic activation of carbon–carbon bonds in cyclopentanones. *Nature* **539**, 546–550 (2016).

74. de Meijere, A. Bonding Properties of Cyclopropane and Their Chemical Consequences. *Angew. Chemie Int. Ed. English* **18**, 809–826 (1979).